A Short Review of Radiation-Induced Degradation of III-V Photovoltaic Cells for Space Applications

Raya-Armenta, José Maurilio; Bazmohammadi, Najmeh; Vasquez, Juan C.; Guerrero, Josep M.

Published in:
Solar Energy Materials & Solar Cells

DOI (link to publication from Publisher):
10.1016/j.solmat.2021.111379

Publication date:
2021

Document Version
Publisher's PDF, also known as Version of record

Solar Energy Materials & Solar Cells 233 (2021) 111379

Contents lists available at ScienceDirect

Solar Energy Materials and Solar Cells

journal homepage: www.elsevier.com/locate/solmat

Review

A short review of radiation-induced degradation of III–V photovoltaic cells for space applications

José Maurilio Raya-Armenta *, Najmeh Bazmohammadi, Juan C. Vasquez, Josep M. Guerrero

Center for Research on Microgrids (CROM), AAU Energy, Aalborg University, Aalborg East, 9220, Denmark

ARTICLE INFO

Keywords:
Review
Photovoltaic cells
Radiation-induced degradation
Space
Future trends
Mathematical modeling approaches

ABSTRACT

The growing interest in space exploration demands exploring new energy resources as well as improvement of the existing sources of energy used in space environments in terms of robustness, reliability, resiliency, and efficiency. This especially applies to the photovoltaic (PV) systems that are required to work efficiently in very hostile environments of radiation under extreme temperatures and vacuum conditions to name a few. In this respect, many efforts have been made to enhance III–V PV-cells technologies towards lighter and more efficient cells. Besides, especial interest has been expressed in understanding and modeling the degradation mechanisms of PV-cells due to the radiation of particles, such as electrons and protons, aiming to improve their radiation resistance. Therefore, an in-depth analysis of the conducted experiments and developed mathematical approximations with updated information is highly useful to guide the research efforts towards the current challenges in the field. In this regard, this paper aims to provide a chronological review of papers published between the 1990s up to the present discussing their main outcome and providing useful information about the experiments and simulation analysis carried out by such studies. The goal is to contribute to understanding the degradation mechanisms of III–V PV-cells caused by the radiation of nuclei particles, as well as to identify the remaining challenges that should be dealt with to improve the current III–V PV technologies for future deep space explorations.

1. Introduction

The growing interest during the last years in outer space missions is forcing governments, international organizations, enterprises, and research institutions to explore more advanced space technologies. This is extremely important not only for optimizing the space trips, but also to ensure the crew and spacecraft safety, especially for some of the most ambitious missions, which are currently ongoing or under development. For instance, the Starlink fleet by SpaceX comprised of 12 thousand small satellites, the new Perseverance rover sent to Mars by NASA, the European rover by the ESA ExoMars programme, the James Webb Telescope by the NASA-ESA-CSA collaboration, crewed missions to Mars by SpaceX, and the recently announced International Lunar Research Station (ILRS) by the cooperation of CNSA and ROSCOSMOS, among many others. Thus, even though the R&D should cover the whole range of technologies, careful attention should be given to the energy source devices, which the entire mission depends on. In this regard, PV technology is a promising technology that has been considered as the main source of energy for space missions relatively near to the Sun since the beginning of the space age in the 1950s. However, outer space is a hostile environment featuring intense particle radiation, ultraviolet irradiation, micro-meteorites, space debris, extreme temperature cycles, vacuum, and electrostatic fields, causing degradation of the PV-cells [1]. Such a degradation is characterized by a gradual deterioration of the PV-cells performance and efficiency. As a result, the PV-cells lifetime will be reduced, which adversely affects the mission cost and time duration [2].

Even though the PV-cells in a space environment are degraded due to different reasons, the degradation due to the exposure to strong particle radiation is one of the major concerns of PV manufacturers and space research societies considering the severe damages that can be caused by it. Near the Earth, this represents a big challenge to satellites given the presence of trapped electrons and protons by the geomagnetic field, particles expelled by solar flares, and galactic cosmic rays (GCRs) to a lesser extend,[1] see Fig. 1.

The radiation-induced degradation of PV-cells is due to the defects created by ions or nuclei particles that strike the solar cells' wafers.

* Corresponding author.
E-mail addresses: jmra@energy.aau.dk (J.M. Raya-Armenta), naj@energy.aau.dk (N. Bazmohammadi), juq@energy.aau.dk (J.C. Vasquez), joz@energy.aau.dk (J.M. Guerrero).

[1] The AP8 and AE8 models are widely-used to describe the entire spectrum of trapped protons and electrons, respectively [9,46,61].

https://doi.org/10.1016/j.solmat.2021.111379
Received 14 May 2021; Received in revised form 24 August 2021; Accepted 1 September 2021
Available online 14 September 2021

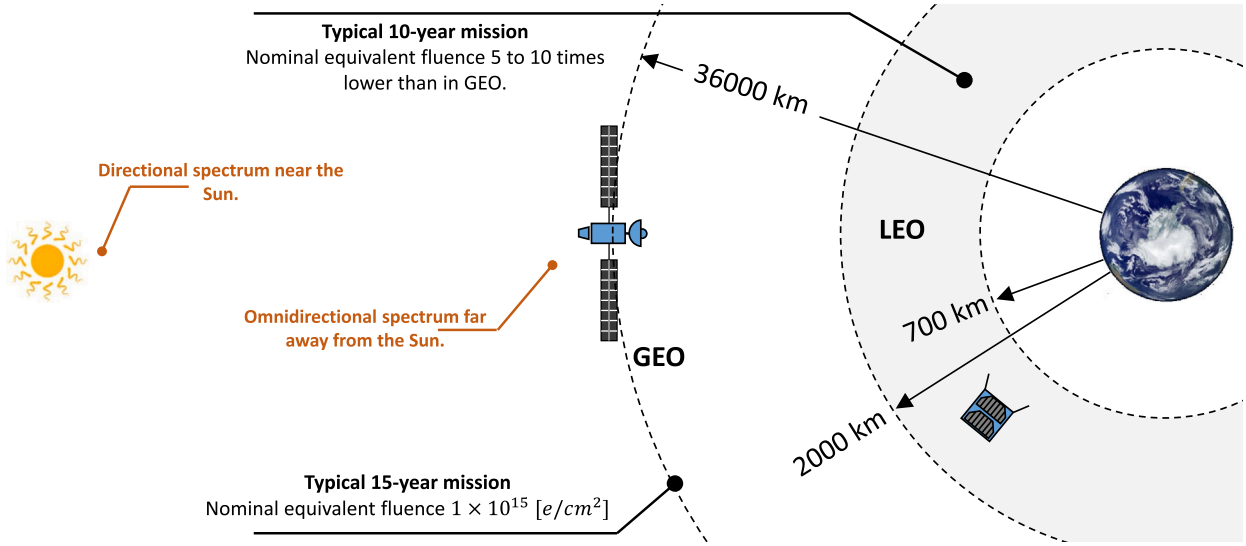

Fig. 1. Illustration of the low earth orbit (LEO) and geostationary earth orbit (GEO) with typical equivalent fluences [3–7]. The spectrum near the Earth is considered omnidirectional, except for solar flare times when the particles direction will be ruled by the geomagnetic lines. Near the Sun, the spectrum is directional since the several scattering processes do not have enough time to fully create omnidirectionality [8].

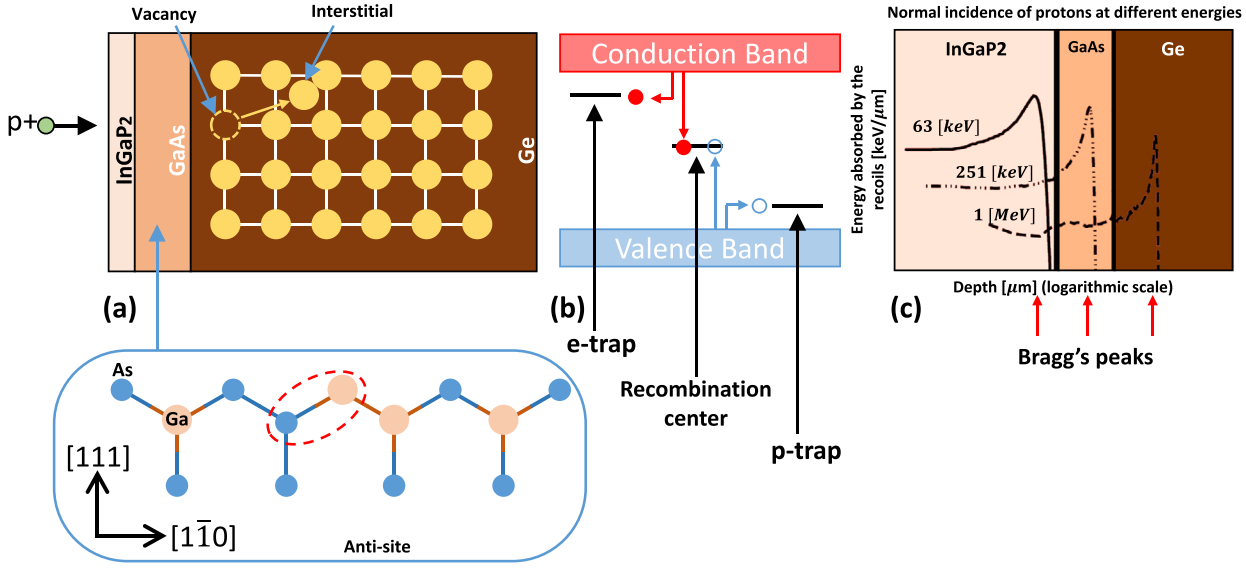

Fig. 2. (a) Graphical representation of a triple-junction (TJ) PV-cell radiated by protons. The radiation-induced degradation is mostly due to atomic displacements (such as vacancies, interstitials, or anti-sites). (b) The defects create levels in the otherwise forbidden bandgap, which might act like minority-carrier traps, majority-carrier traps, recombination centers, generation centers, or temporary trapping centers [5,12,13]. (c) Profile of energy absorbed by recoils due to different streams of mono-energetic and unidirectional (normally incident) protons using SRIM [8].

The striking particles modify the crystal structure of the semiconductors by ionization or atomic displacements, see Fig. 2-(a). The latter is the most damaging degradation mechanism given that it creates defects in the crystal that negatively affect the carriers in the energy bands. The defects might act like trapping, generating, or recombination centers, depending on the location of the defect's energy level in the bandgap, see Fig. 2-(b). Besides, the recombination centers reduce the diffusion length while the trap centers decrease the net amount of carriers (the carrier removal effect) [4]. In general, the degradation due to the particle radiation mostly depends on the sort of particle, its energy and impacting direction, the material of the cell, the active region thickness, and the concentration and type of doping [8,9]. For instance, it has been stated that a 1 [MeV] electron impacting a Ge wafer generates on average a Frenkel pair, *i.e.*, a vacancy and an interstitial, while one proton with the same energy creates clusters of damage (3000 times more damage than the electron regarding the threshold energy of 15 eV) due to the larger density of collision events [10,11]. Besides, particles that strike normally with low-enough energy get trap inside the cell and present a damage profile with a peak at the end of the range, named "Bragg peak", where the largest damage is located, see Fig. 2-(c). This indicates a non-uniform minority-carrier lifetime across the cell and consequently a non-uniform degradation [8,10].

The effects caused by particle radiation that adversely affect the PV-cells have been identified by several studies. Some important effects are summarized in Table 1. The reader is referred to the reference list to see the very specific conditions at which such effects appear.

In this respect, several methods to reduce the radiation effects on PV-cells have been proposed. For instance, thermal annealing [22], illumination exposure [24], forward bias [24] for recovering, whereas coatings [25], nano-structures [26], Bragg reflectors (BRs) [27], for hardening, *etc.* Besides, including a cover glass can reduce the level of radiation exposure due to the shielding effect. Accordingly, it has

Table 1
Effects of the radiation-induced degradation on the III–V/Si PV-cells.

Effect	References
Reverse saturation current increase, except for very low temperatures.	[14–16]
Anomalous short-circuit current and open-circuit voltage degradation (Si PV-cells) and series resistance increment. Explained by a minority-carrier diffusion length shortening (or minority-carrier lifetime reduction), depletion region broadening, and base carrier concentration decrease.	[12,17]
Base layer doping type shift.	[12,15]
The surface recombination velocity (SRV) increases (surfaces and interfaces).	[4,18,19]
Minority-carrier lifetime reduction.	[20]
Short-circuit current, open-circuit voltage, and maximum power decrease.	[13]
The current-voltage (IV)-characteristics slope (from zero to the maximum power point (MPP) voltage) becomes steeper.	[5,21]
Decrease of the external quantum efficiency (EQE). The longer the wavelength region, the more severe the damage. The higher the energy of the particles (regarding particles stopping inside the cells), the more severe the damage in the longer wavelength region.	[14,21,22]
Appearance of *artifacts* (UMM PV-cells).	[21]
Reduction of electroluminescence (EL) intensity.	[23]

Table 2
Proposed techniques to reduce the radiation effects in III–V/Si PV-cells.

Technique	References
Base-carrier concentration optimization.	[24,29]
Top layer's base thickness optimization (double junction (DJ)).	[24]
Use of current-limiting layer by the hardest material to radiation.	[30,31]
Coverglass thickness optimization.	[8,25]
Use of i-layers between the pn junctions.	[32]
Increase the fraction of In and P in the layers composition.	[13,22]
Use of two thin and highly doped configurations: Shallow junction *p*-type base, and deep junction *n*-type base.	[6]
Use of ultra-thin and highly-doped configurations.	[6]
Use of TF PV-cells with back reflector and shallow junction.	[4]
Use of lowly-doped and passivated Ge-based subcells.	[10]
Use of GaInP instead of AlGaAs to build the BSF.	[33]
Narrowing the BSF thickness.	[34]
Use of shallow junctions not only in substrate-based, but also in TF-based PV-cells.	[7]
Use of nano-structures.	[26]
Use of BRs while the sub-layers are thinned.	[35–37]

been stated that a fused silica coverglass of about 75 μm is able to stop electrons and incident protons with energies lower than 200 keV and 2.8 [MeV] respectively while the higher energetic particles are slowed down [25,28]. In addition, systems used for concentrating sunlight might support not only the increase of cell efficiency, but also the radiation shielding. However, for space applications, it is advised to use no larger than 50 suns concentrations due to the difficulty of handling high temperatures [3]. Besides, thin-film (TF) technology has been proven to be very promising for space applications due to its low specific mass, high specific power, and radiation hardness [4,8]. Even, it has been suggested that a diffusion length of three times the wafer thickness, on Ge, ensures a high quantum efficiency (QE) after radiation [10]. Moreover, the III–V multi-junction (MJ) architectures have been proposed for space applications due to their high efficiency and radiation hardness, see Fig. 3. A summary of important techniques proposed to reduce the effects of the radiation-induced degradation is given in Table 2.

Although a great deal of effort has been put into radiation-induced degradation analysis of PV-cells over the last decades, still there exist many issues to be overcome for the efficient and vast deployment of PV system technologies for space applications. Moreover, further investigations for boosting PV-cells efficiency and prolonging their lifetime by slowing down the degradation process are required. Therefore, more studies dedicated to understanding and modeling of the radiation-induced degradation mechanisms of PV-cells as well as efficient techniques for recovering and hardening of PV-cells against radiation are required. Besides, there exists the need for updated review studies to help researchers keep track of the new findings and significant challenges.

To the best of our knowledge, only a few review studies have been fully dedicated to analyzing the radiation-induced degradation of III–V/Si-based PV-cells, while others partially address the topic. For instance, in 1975, a review of the Si-based PV-cells damage due to the proton and electron radiation was reported [40]. Afterwards, a review study dedicated to the InP-based PV-cells was published in 1988 with a discussion of radiation hardness and a comparison with Si and GaAs solar cells [41]. Then, in 1991, the TF architecture was reviewed from the radiation-induced degradation point of view [42]. Three years later, in 1994, the radiation effects upon InP-based PV-cells were analyzed in [43]. Since then, no major review study specific to the radiation-induced degradation of PV-cells has been reported in the literature. In a recent study, published in 2021, a review study dedicated to classifying different kinds of MJ III–V PV-cells was published while an introduction to the radiation-induced degradation of PV-cells was given and the Jet Propulsion Laboratory (JPL) and Naval Research Laboratory (NRL) methods to characterize radiated PV-cells were introduced [44].

Therefore, this paper aims to provide a chronological overview of the radiation-induced degradation studies of III–V PV-cells, reviewing the proposed physical–mathematical degradation modeling approaches while emphasizing the most recent studies. The most important conclusions and remarks of the reviewed studies are discussed to provide an in-depth understanding of the radiation effects upon the performance of the solar cells. In addition, different architectures and technologies of III–V PV-cells are thoroughly reviewed and practical information about the conducted degradation analysis, simulations, and experiments are given. Finally, the remaining topics that require more investigation are identified. Thus, this review paper is paving the way for the new studies by providing a solid starting point to further analysis of radiation-induced degradation of PV-cells and enhance their performances for space applications.

The rest of this paper is organized as follows. In Section 2, a chronological review of different studies dedicated to the radiation-induced degradation analysis of PV-cells is provided. Then, in Section 3, important remarks and significant challenges that are remaining open for more investigation are identified. Concluding remarks are given in Section 4. And finally a general description of the mathematical variables is given in Appendix.

2. Review of radiation-induced degradation of PV -cells studies

This section is devoted to give a chronological review of different studies dedicated to the degradation process of PV-cells due to the bombarding of energetic particles. The review starts with the traditional Si wafers used for space applications in the 1950s and ends with the next-generation III–V MJ PV-cells studied in the present. A time-line of the reviewed studies from 1991 up to the present is given in Fig. 4. Besides, at the end of this section, the main characteristics of the reported experiments are summarized in Table 3. It should be noticed that a brief description of each variable presented in the following mathematical expressions are either provided in the text or Appendix.

2.1. Initial efforts in space PV -cells

The 1950s was the decade in which the PV-cells started to be considered the most reliable medium to supply energy to spacecrafts with efficiencies of barely 7%–8% (Si). The improvements came with

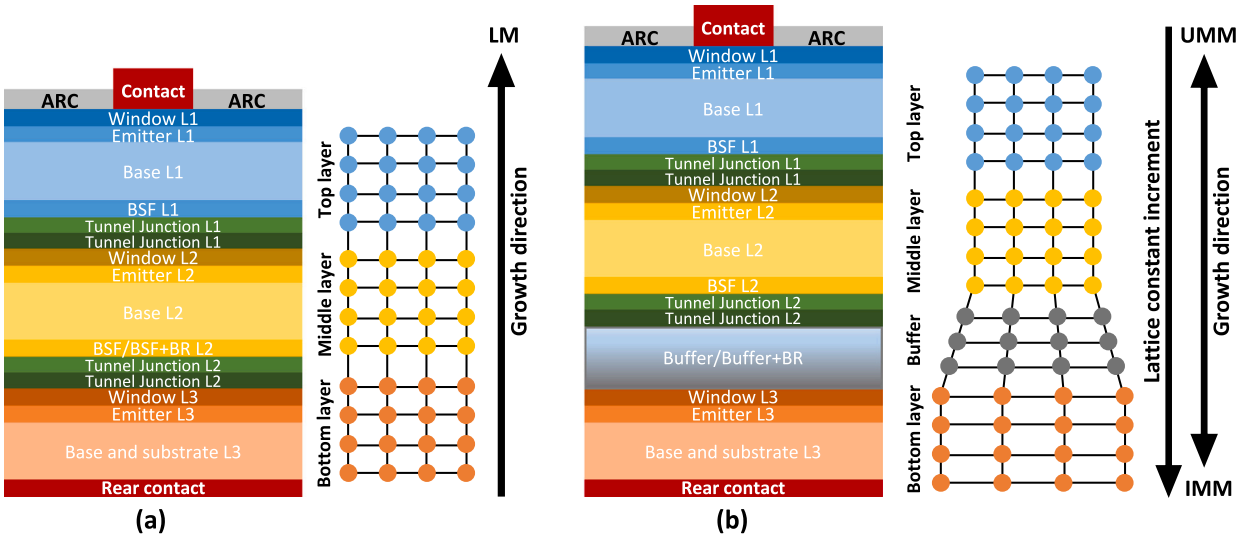

Fig. 3. (a) Schematic representation of a TJ lattice-matched (LM) PV-cell. GaInP/GaAs/Ge is the most widely-used in space applications due to its high efficiency (~30%), matured manufacturing technologies, and radiation hardness [14]. However, the mismatch among their photo-generated current makes the bottom layer to work at a non-optimum point [21]. (b) Schematic representation of a TJ PV-cell, UMM and inverted metamorphic (IMM). These architectures are proposed to optimize the bandgap matching among the layers while using materials of different lattice constants. Some UMM PV-cells have been recently proposed with efficiency around 40% for terrestrial applications and sunlight concentration [14,38,39].

architecture changes, introduction of the BSF, BRs, and anti-reflective coatings (ARCs), as well as the introduction of III–V compounds like GaAs and InP. More improvements came with the introduction of MJ architectures, which were much more efficient than the Si-based PV-cells and some even more cost competitive, see Fig. 5.

2.2. Studies from 1991 to 2000

Being a pioneer in studies of radiation, the JPL laboratory reported the damage coefficients for GaAs/Ge solar cells corresponding to the bombarding of electrons and protons in 1991 [45]. Such coefficients are used to estimate experimentally the degree of degradation of a PV-cell due to bombarding of protons and electrons by means of the fluence equivalent method (an introduction to this method is given later in this section, see [9]). The energy of electrons was 0.6, 1.0, 2.4, and 12 [MeV], at the room temperature (RT), except for the highest energy for which temperatures between 49 °C and 88 °C have been reported. On the other hand, the energy of protons was 0.05, 0.2, 0.3, 0.5, 1.0, 3.0, and 9.5 [MeV] at RT. All the tests were performed under vacuum condition where the cells were front-shielded by glasses with different thicknesses (0–60 mils) and it was assumed that they are back-shielded with an infinitely thick glass. The results show the average damage coefficient profiles vs the fluence for the maximum power, short-circuit current, and open-circuit voltage of 4 to 5 solar cells. Besides, according to the authors, after the comparison of two GaAs-based PV-cells, there was a very small difference in the degradation due to proton bombarding between the two kinds of cells for energy levels of higher than 100 [keV]. Particles with lower energies get stuck inside the shielding or the semiconductor material, which show different profiles for the degradation coefficients according to the presented results.

Still in 1991, the use of BRs to improve the efficiency and radiation tolerance of GaAs PV-cells was introduced in [27]. Alternating layers with material of different refractive indices were used to achieve very high levels of reflection in specific wavelength ranges. The thickness of each layer, t_1 and t_2, for the wavelength of design, λ, were given as

$$t_1 = \frac{n_1 \lambda}{4}, \qquad t_2 = \frac{n_2 \lambda}{4}, \tag{1}$$

while the material used for the BR was $Al_xGa_{1-x}As$, which reduces the refractive index monotonically with x. It was determined that more than fifteen periods can produce reflectances of about 100%, allowing to have thinner cells with similar current densities. However, the thickness of the cell is limited by the restricted spectral width of a single reflector. Thus, a multi-reflector with different peak wavelengths can be implemented to reduce such a limitation at a cost of having a thicker wafer according to the authors. It was shown that these BRs would be more effective in 1 than 2 and 3[μm] cells. Nevertheless, single reflectors with eight and fifteen periods with 1 and 2[μm] of thickness were implemented showing an improved PV-cell efficiency of up to 0.7%. Besides, the improvement of the EQE for the high wavelength region was presented.

Later in 1996, the JPL released a very complete report about the degradation effects due to electrons and protons in GaAs-based PV-cells [46]. The report includes an overview of the physical fundamentals of radiation-induced degradation mechanism of GaAs-based PV-cells, experimental techniques for characterization of the cells, and the radiation effects, among others. Besides, complete profiles of the short-circuit current, open-circuit voltage, maximum power, *etc.*vs the fluence of 1 [MeV] electrons are provided in the corresponding units and normalized for different GaAs-based PV-cells. Moreover, plenty of tables and continuous curves (fitted to experimental data by least-square method) with experimental data regarding the radiation-induced degradation dependency with temperature and solar irradiance of different parameters of the GaAs-based PV-cells are provided. The temperature ranges from −120 to +140 °C, the solar irradiation from 50 to 2500 [W/m^2], and the radiation fluences of 0, 1×10^{14}, and 1.1×10^{15} [e/cm^2] electrons having energy of 1 [MeV]. The temperature during the particle radiation was kept at RT. Previous to the radiation, an increase of the short-circuit current with the increase of temperature is shown for all solar irradiance levels, whereas a much more sharp reduction of the open-circuit voltage, resulting in a reduction of the maximum power with the increment of temperature for all solar irradiance levels. The short-circuit current and open-circuit voltage are shown to increase with the solar irradiance when the temperature is kept constant, resulting in an increment of the maximum power for all the temperatures. On the other hand, after the radiation, the parameters follow the same trend while having lower magnitudes.

The first generation of space solar cells was comprised of Si wafers given their good trade-off between efficiency and cost. Nevertheless, earlier studies showed a gradual degradation of these cells caused

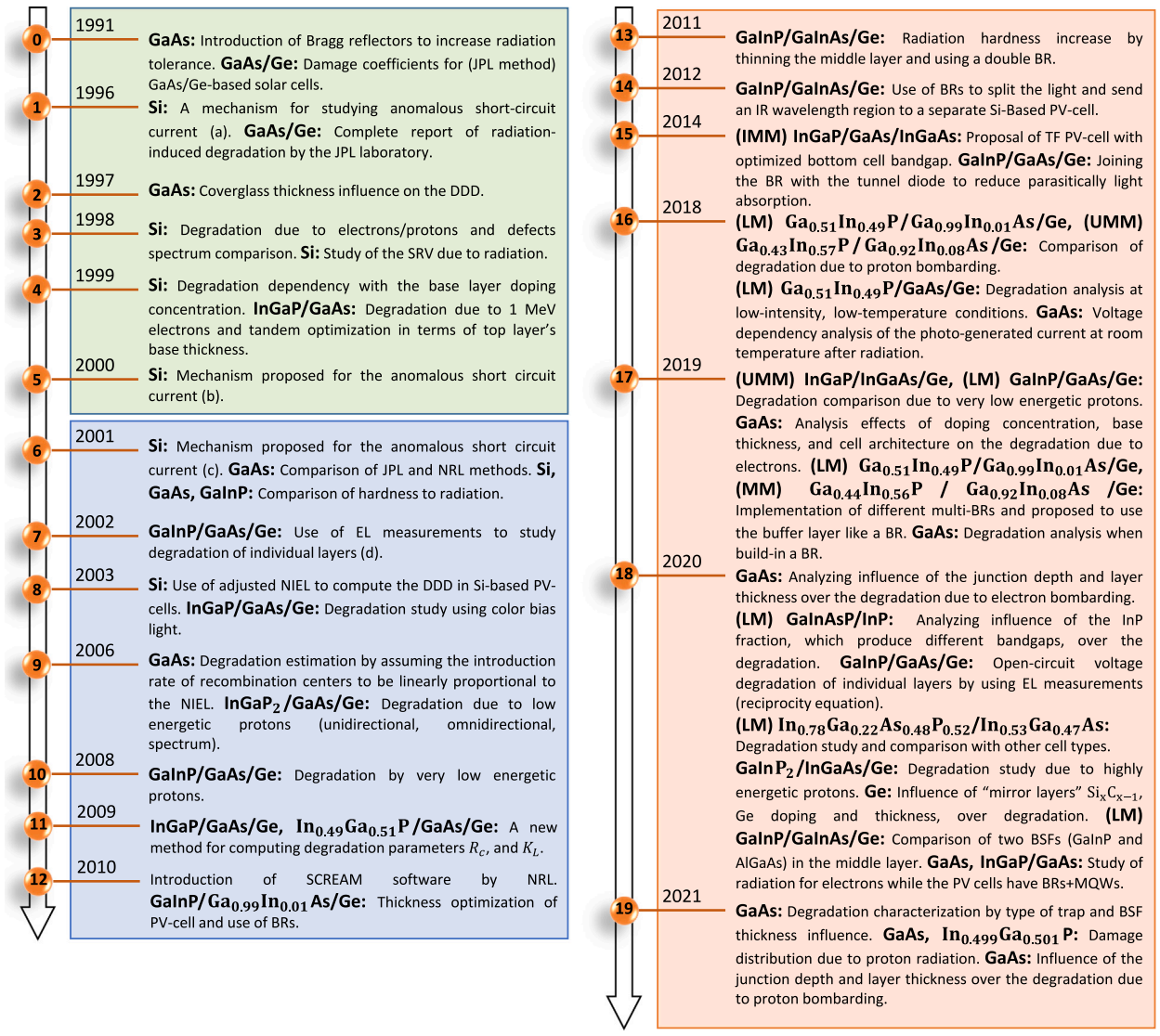

Fig. 4. Timeline of studies dedicated to the degradation of PV-cells due to nuclei particles bombarding. 0: [27,45]. 1: [17,46]. 2: [25]. 3: [12,18]. 4: [24,29] 5: [15]. 6: [9,47,48]. 7: [30]. 8: [49,50]. 9: [8,51]. 10: [11]. 11: [19,20]. 12: [28,52]. 13: [35]. 14: [53]. 15: [32,54]. 16: [5,13,16]. 17: [6,21,36,55]. 18: [4,10,14,22,23,33,37,56]. 19: [7,34,57]. Notes: (a) Based on depletion broadening, carrier removal, and diffusion length shortening. (b) Based on the Shockley–Read-hall (SRH) theory and electroneutrality. (c) Based on the SRH theory, electroneutrality, and considering deep traps. (d) The decrease of luminescence intensity is analyzed.

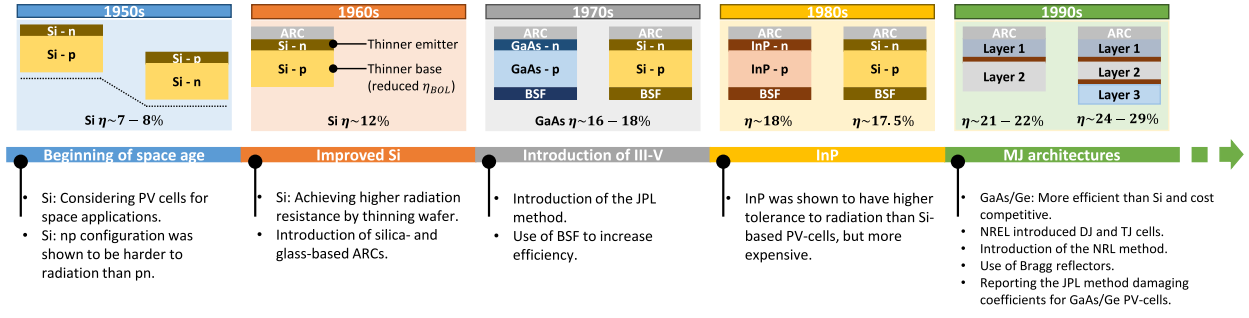

Fig. 5. Time-line of the PV technology from 1950s up to the beginning of 1990s [9,25,27,45,58,59].

by relatively low fluences, followed by an anomalous short-circuit current increment at a localized fluence just before a sudden failure. Accordingly, a mechanism for modeling such an anomalous behavior in a BSF Si PV-cell radiated by electrons was proposed in [17] in 1996. For the gradual degradation, the minority-carrier diffusion length shortening was given as

$$\Delta\left(\frac{1}{L^2}\right) = \frac{1}{L_\phi^2} - \frac{1}{L_0^2} = \sum \frac{I_{ri}\sigma_i \upsilon \phi}{D} = K_L \phi, \tag{2}$$

where the suffixes 0 and ϕ mean before and after the radiation, respectively. The diffusion length shortening is due to the creation of

Table 3
Characteristics of carried out experiments.

Type of cell	Particle	Energy [MeV]	Fluence #/cm^2 DDD [MeV]/g	Flux #/(cm^2 s)	Spectrum	Method	Temp.	Software	Ref.
Si	Electron	1	10^{14}–10^{17}	N.S.	AMO	C-V[1]	RT	N.S.	[17]
Si	Electron Proton	1 10	3.2×10^{12}–9.5×10^{16} 5×10^{9}–1.5×10^{14}	N.S.	N.S.	C-V[1], Hall meas.[2], IV[2], DLTS[3]	RT	N.S.	[12]
Si	Proton	3 and 10	1×10^{11}–2×10^{14}	N.S.	AMO	N.S.	RT	PC1D[4]	[18]
Si	Electron	1	0-10^{18}	N.S.	AMO	N.S.	RT	PC1D	[29]
Si	Any	N.S.	N.S.	N.S.	N.S.	N.S.	RT	N.S.	[15]
Si	Electron Proton	1 10	N.S.	N.S.	N.S.	N.S.	RT	N.S.	[47]
Si	Proton	0.1–10	DDD 10^{8}–10^{12}	N.S.	AMO	N.S.	RT	SRIM[5]	[49]
GaAs	Proton	1–400	DDD 10^{8}–2.5×10^{10}	N.S.	AMO	N.S.	N.S.	SRIM	[25]
GaAs	Electron Proton	1 1	10^{12}–10^{16} 10^{9}–10^{12}	N.S. N.S.	AMO AMO	Dark IV[7], DLTS[8], I_{sc}&V_{oc}[9], EL[8]	N.S. N.S.	N.S. N.S.	[51]
GaAs	Electron Proton	1 and 3 1	1×10^{14}–2×10^{16} 5×10^{10}–1×10^{13}	1.5×10^{12} 1.9×10^{9}- 5.7×10^{10}	AMO	IV[15], dark IV[35], C-V[1], SR[23]	RT	N.S.	[5]
GaAs	Electron	1	1×10^{15}	N.S.	N.S.	N.S.	N.S.	N.S.	[6]
GaAs	Electron	1	1×10^{13}–1×10^{15}	5×10^{11}	AM1.5, AMO	IV[15], SR[13] Dark IV[20]	RT	N.S.	[4]
GaAs	Proton	1	10^{11}–10^{13}	N.S.	AMO	IV[15] (simulation)	N.S.	SCAPS[32]	[34]
GaAs	Proton	1	5×10^{10}–2×10^{11} 5×10^{11}–5×10^{12}	1×10^{9} 1×10^{10}	N.S.	IV[15], dark IV[35], SR[13]	RT	N.S.	[7]
GaAs, Ge	Electron Proton	0.6–12 0.05–9.5	DDD 10^{7}–3×10^{11} DDD 10^{7}–10^{11}	N.S.	AMO	JPL/NRL	N.S.	SRIM[5]	[9]
Ge	Electron Proton	1	3×10^{13}–1×10^{16} 1.33×10^{10}–1.33×10^{11}	5×10^{11}	N.S.	μW-PCD[33]	RT	SRIM[12]	[10]
Si, GaAs, GaInP	Electron	1	0-5×10^{16}	N.S	AMO	C-V[1]	RT	N.S	[48]
GaAs, $In_{0.499}Ga_{0.501}P$	Proton	1–8	~ 10^{15}	2×10^{12}	N.S.	RS[6], PLS[26]	RT	SRIM[6]	[57]
InGaP/GaAs	Electron	1	3×10^{14}–1×10^{16}	10^{12}	AMO	J_{sc}[34]	RT	N.S.	[24]
LM GaInAsP/InP	Electron	1	3×10^{14}–3×10^{15}	N.S.	AMO	X-ray diffraction[21], ECV[22], SR[23], IV[15]	RT, 60[24]	TCAD Sent[25]	[22]
LM $In_{0.78}Ga_{0.22}As_{0.48}P_{0.52}/In_{0.53}Ga_{0.47}As$	Electron Proton	1 3, 10	DDD 3.16×10^{9}- 3.16×10^{10}	1×10^{11} 2×10^{8}	AMO	IV[15], SR[13]	RT	MULASSIS[27] CASINO[28], SRIM[14]	[14]
GaInP/GaAs/Ge	Electron	1	1×10^{14}–4×10^{15}	N.S.	N.S.	EL	RT	N.S.	[30]
InGaP/GaAs/Ge	Proton	0.03–10	10^{10}–10^{14}	N.S.	AMO	SR	N.S.	TRIM[6]	[50]
$InGaP_2$/GaAs/Ge	Proton	0.03–5	DDD 10^{8}–10^{12}	N.S.	AMO	N.S.	RT	SPENVIS[10] MULASSIS[11] SRIM[12]	[8]
GaInP/GaAs/Ge	Proton	0.28–2.80	10^{10}–10^{13}	5×10^{8}	AMO	IV[15], SR[13]	RT	SRIM[14]	[11]
InGaP/GaAs/Ge	Electron Proton	1–2 0.03–10	3×10^{16} 10^{12}–10^{14}	N.S.	AMO AMO	N.S.	N.S.	PC1D[4]	[19]
$In_{0.49}Ga_{0.51}P$/GaAs/Ge	Proton	0.03–10	10^{12}–10^{14}	5×10^{10}	AMO	IV[15], SR[13]	N.S.	PC1D[4]	[20]
IMM InGaP/GaAs/InGaAs	Electron	1	0-3×10^{15}	N.S.	AMO	N.S.	RT	N.S.	[32]
LM $Ga_{0.51}In_{0.49}P/Ga_{0.99}In_{0.01}As$/Ge UMM $Ga_{0.43}In_{0.57}P/Ga_{0.92}In_{0.08}As$/Ge	Proton	3 and 8	DDD 1.91×10^{9}- 5.73×10^{10}	1.1×10^{9}- 1.3×10^{9}	AMO	X-ray diffraction[16], Cathodoluminescence[17]	RT	SRIM[14]	[13]
GaInP/$Ga_{0.99}In_{0.01}As$/Ge	Electron	1	10^{15}–3×10^{15}	–	–	–	–	–	[52]
LM $Ga_{0.51}In_{0.49}P$/GaAs/Ge	Proton	1	2×10^{10}–1.6×10^{12}	4×10^{9}	AMO[18]	IV[15]	100-300 K	SRIM[12]	[16]
UMM InGaP/InGaAs/Ge LM GaInP/GaAs/Ge	Proton	0.05, 0.15	5×10^{10}–8×10^{11} 5×10^{10}–1×10^{12}	N.S.	N.S.	IV[15], SR[13]	N.S.	SRIM[14], wxAMPS[19]	[21]
GaInP/GaAs/Ge	Electron	1	3×10^{13}–1×10^{15}	5×10^{10}	N.S.	EL[26]	RT	N.S.	[23]
$GaInP_2$/InGaAs/Ge	Proton	24.5	DDD 0-1.06×10^{12}	N.S.	AMO	IV[15], dark C-V[1], dark C-F[30], dark G-F[31]	RT	SRIM[29]	[56]
GaInP/GaInAs/Ge	Electron	1	10^{14}–10^{16}	1×10^{11}	AMO	X-ray diffraction[21], IV[15], SR[13]	< 50^{o}C	N.S.	[33]
GaInP/GaAs/$Ga_{0.7}In_{0.3}As/Ga_{0.42}In_{0.58}As$	Electron Proton	1 0.17	1×10^{13}–2×10^{15} 1×10^{11}–3×10^{12}	N.S.	AMO	IV[15], SR[13]	RT	TCAD[25], CASINO[28], MULASSIS[27], SRIM[6]	[31]

1: Method to measure the carrier concentration and built-in voltage. 2: To perform the base layer resistivity. 3: To determine the energy level of the induced defects at different temperatures. 4: To get the EQE. 5: non-ionizing energy loss (NIEL) computation. 6: Proton ranges. 7: $I_{ri}\sigma$. 8: I_{ri}. 9: Average $I_{ri}\sigma$. 10: To obtain the differential proton spectrum of a highly elliptical orbit (HEO) on Earth. 11: To corroborate the slowed down spectrum of protons. 12: Energy absorbed by the recoils along the path of the particles inside the cell in [keV/μm] or the energy absorption rate in [eV/Angstrom-Ion]. 13: To compute the QE at different fluences and energies. 14: Irradiation-induced vacancies. 15: To compute I_{sc}, V_{oc}, P_m, IV-characteristics, fill factor (FF). 16: To estimate the strain among layers. 17: To estimate dislocations density. 18: Jupiter conditions 3.7% AMO. 19: To compute the recombination rate distribution. 20: To estimate V_{oc}. 21: To measure lattice constant. 22: To estimate doping concentration. 23: To measure EQE and derive the bandgap or diffusion lengths. 24: For the regeneration experiments. 25: Optical and electrical modeling. 26: To estimate the relative luminescence degradation of intensity. 27: To compute the DDD, NIEL. 28: To estimate electrons trajectory. 29: To estimate displacement damage distribution and particles trajectory. 30: To compute the capacitance contribution due to the interface traps. 31: To estimate the interface trap density and trap time constant. 32: Software developed at the University of Gent. 33: To measure the minority-carrier lifetimes. 34: Before and after annealing to estimate annealing rates. 35: To estimate saturation currents, ideality factor.

recombination centers during the radiation, which reduces the likelihood of a minority carrier to get collected. The anomalous short-circuit current increase was explained by a depletion region broadening, which would increase the contribution of the depletion region to the short-circuit current and thereby the open-circuit voltage reduction. The proposed expressions were as follows

$$J_D = 1 - \exp(-\alpha W), \tag{3}$$

$$V_{oc} = \frac{nkT}{q}\ln\left(\frac{J_{sc}}{J_0}+1\right), \tag{4}$$

$$J_0 \propto qDWn_i/2L^2. \tag{5}$$

And finally, the sudden failure by a reduction of the carrier concentration in the p-type base was modeled as

$$\Delta p = p_0 - p_\phi = \sum I_{tj} f(E_{tj})\phi \approx R_c \phi, \tag{6}$$

$$p_\phi = p_0 \exp\left(-R_c\phi/p_0\right), \tag{7}$$

which results in a rise of the resistivity consequently. This virtual reduction of carrier concentration has been explained by the increase of trap centers. The modeling approach followed the experimental data profile.

Later in 1997, authors in [25] studied the impact of the coverglass thickness on the displacement damage dose (DDD) introduced to GaAs PV-cells due to radiation of protons. According to the results, the thinner the coverglass, the larger the damage to the PV-cell. Besides, an increase of the displacement damage was found by decreasing the protons' energy until reaching a maximum level close to the threshold of the atomic displacement. The particles trajectory was assumed straight through the coverglass while their energy was obtained using the particle range, $R(E)$, as follows

$$R(E) = AE^a + BE^b. \tag{8}$$

By using the continuous-slowing down approximation, it is assumed that particles traveling through the material do not encounter any nuclei (zero nuclear stopping power), which otherwise would produce the particles to be scattered. Instead, the particles are assumed to be stopped continuously by a homogeneous "electrons cloud" without a change in their trajectory (electron stopping power). The incident spectrum, $g(E)$, was proposed to shift to a slowed-down spectrum, $f(\epsilon)$, as

$$f(\epsilon) = g(E)\frac{dE}{d\epsilon}. \tag{9}$$

Similarly, in 1998, authors in [12] used the DDD approximation to study the degradation of Si-based PV-cells due to the bombarding of electrons and protons with different energy levels. The minority-carrier diffusion length was expressed by (2) and the majority-carrier concentration by (6) while a double-diode (DD) model was used to represent the PV-cell. In addition, the width of the depletion region was considered as follows

$$W = \sqrt{\frac{2\left(V - V_{bi}\right)\epsilon_0\epsilon}{qp}} \tag{10}$$

and the saturation current densities were computed using (2), (6), and (10) as

$$J_{01} = \frac{qD_n n_i^2}{Lp}, \rightarrow J_{01,\phi} = J_{01,0}\sqrt{K_L L_0^2\phi + 1}\,\frac{p_0}{p_0 - R_c\phi}, \tag{11}$$

$$J_{02} = \frac{qWD_n n_i}{2L_{eff}^2}, \rightarrow J_{02,\phi} = J_{02,0}\left(K_L L_0^2\phi + 1\right)\sqrt{\frac{p_0}{p_0 - R_c\phi}}, \tag{12}$$

where $J_{01,\phi}$ represents the ideal saturation current density in the base layer while $J_{02,\phi}$ is the generated saturation current density integrated in the space charge region, both after being radiated by a fluence ϕ. Using IV-characteristics curve fitting and hall measurements, an increase in the resistivity of the base layer was observed with the increase of DDD. Nevertheless, the theoretical results were not accurate-enough since only the increase of carrier concentration was considered. It was suggested that further DDD might produce a shift of the doping type in the base layer. Finally, regarding the spectrum of energy levels found, the protons were producing deeper defects that ease the carriers recombination.

During the same period, the effect over the SRV due to proton radiation of Si PV-cells was investigated in [18]. Essentially, the study suggested an increment of the SRV with the proton fluence. Here, the anomalous short-circuit current degradation due to radiation was also perceived. Thus, (2) was used for modeling shortening of the diffusion length, (6) for the majority-carrier concentration change, and (3), (4), and (5) for the depletion region broadening. The simulation results followed the experimental data profile, whereas the QE presented inaccuracies at the short-wavelength region.

In 1999, the degradation dependency on the base layer doping in Si-BSF PV-cells due to radiation of electrons was investigated in [29] and the same anomalous degradation of short-circuit current and open-circuit voltage was reported. The diffusion length shortening was modeled by (2) and the majority-carrier removal by (6) and (7) while the depletion region broadening was also considered. Besides, an empirical equation was proposed for each type of doping (p-, n-) to represent the damage coefficient of minority-carrier diffusion length, K_L, in terms of the carrier concentration. On the other hand, the majority-carrier removal rate, R_c, seemed to be not dependent on the carrier concentration. The results showed a direct and inverse correlation between the carrier concentration of the base layer and the maximum conversion efficiency, see Table 4. Besides, the authors highlighted that optimizing the carrier concentration of the base layer brings a lower initial diffusion length. Thus, a trade-off between the BOL and EOL should be found.

At that time, authors of [24] presented a study of radiation resistance of the tandem InGaP/GaAs due to the bombarding of 1 [MeV] electrons and its recovery by thermal, illumination, and forward bias injections. The comparison made with InP, InGaP, and GaAs-on-Ge cells indicated that InGaP/GaAs has the lowest remaining factor of the maximum power similar to that of GaAs-on-Ge cells. In addition, the largest power recovery was shown for the highest temperature of 75 °C. However, the annealing recovery in the tandem was much smaller than in single-junction (SJ) InGaP cells. Thus, a tandem optimization in terms of the top layer's base thickness was proposed for current matching, to improve the recovery and radiation resistance. The results indicated an optimal thickness of around 0.2–0.3 [μm]. Finally, it was suggested to reduce the base carrier concentration of both layers to increase the radiation resistance.

Later in 2000, authors in [15] proposed another mechanism for the anomalous increment of the short-circuit current in Si PV-cells while it is radiated by nuclei particles. The formulation is based on the SRH recombination theory and the electroneutrality condition as

$$R_{REC} = \frac{np - n_i^2}{\frac{1}{C_p N_t}(n + n') + \frac{1}{C_n N_t}(p + p')} = \frac{\delta_n}{\tau_n} \rightarrow \tau_n = \frac{1}{C_p N_t}\frac{n + n'}{n_i\frac{\delta_p}{\delta_n} + p} + \frac{1}{C_n N_t}\frac{p + p'}{n_i\frac{\delta_p}{\delta_n} + p}, \tag{13}$$

$$\tau_p = \frac{1}{C_p N_t}\frac{n + n'}{p_i\frac{\delta_n}{\delta_p} + n} + \frac{1}{C_n N_t}\frac{p + p'}{p_i\frac{\delta_n}{\delta_p} + n}, \tag{14}$$

$$n + N_a = p + \frac{N_t\left(C_n n' + C_p p\right)}{C_n(n + n') + C_p(p + p')}, \tag{15}$$

where R_{REC} represents the recombination rate [#/volume-time] of electrons and holes due to the non-radiative recombination centers, $n = n_i + \delta_n$, and $p = p_i + \delta_p$. In addition, the dark saturation current density, the short-circuit current density, and the open-circuit voltage were expressed as

$$J_0 = \frac{qD_n n_i}{L_n}\tanh\left(\frac{W}{L_n}\right), \tag{16}$$

$$J_{sc} = q\Phi\cosh^{-1}\left(\frac{W}{L_n}\right), \tag{17}$$

$$V_{oc} = \left(\frac{kT}{q}\right)\ln\left(\frac{J_{sc}}{J_0} + 1\right), \tag{18}$$

where $L_n = \sqrt{D_n\tau_n}$ and $D_n = \mu_n kT/q$. The simulation results showed an anomalous increase of the minority-carrier lifetime when $N_t \approx N_a$. The suggested responsible mechanism was a sudden reduction in carrier density with an increment in the base layer resistivity. Besides, it was observed how the base layer switched from p-type to n-type when the traps concentration increased.

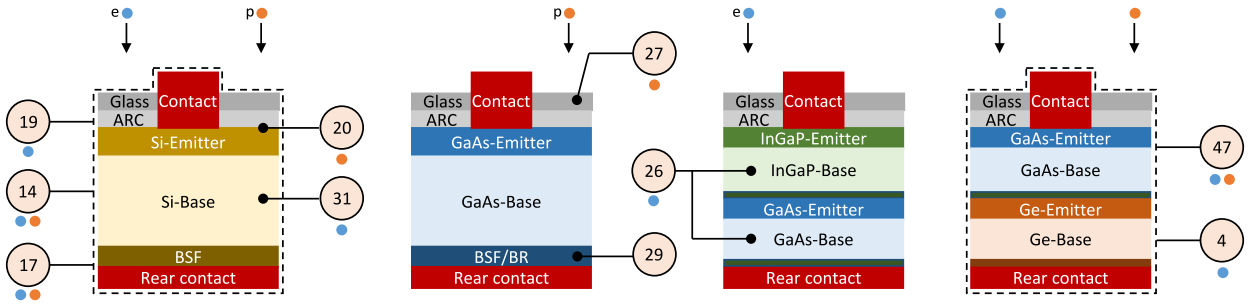

Fig. 6. Type of cells reviewed in this paper for the period 1991 to 2000. The labels indicate the element studied/optimized/compared in terms of radiation resistance by [12,15,17,18,24,25,27,29,45,46]. It should be noticed that the substrate may be present between the BSF and the rear contact.

Fig. 6 provides an illustrative representation of the different PV-cell architectures studied by the articles reviewed in this paper for the period 1991 to 2000. The element of the cell under analysis and the kind of particle used for the respective study are indicated.

2.3. Studies from 2001 to 2010

In 2001, authors in [47] also reported an anomalous increase of the minority-carrier lifetime with respect to the majority-carrier lifetime on Si-based PV-cells due to bombarding of electrons and protons. This approximation was also based on the SRH recombination theory (13), (14), and the electroneutrality condition (15) while it was assumed that the induced traps are located close to the middle of the bandgap (intrinsic Fermi level). The statistical factors were expressed as

$$n' = N_c \exp\left(-\frac{E_t}{kT}\right), \tag{19}$$

$$p' = N_v \exp\left(\frac{E_t - E_g}{kT}\right), \tag{20}$$

while the reverse saturation current density, short-circuit current density, and open-circuit voltage were computed by (16), (17), and (18), respectively.

At the same time, the methods proposed by the JPL and NRL, to estimate the degradation of PV-cells were compared in [9]. One important advantage of the NRL method is the reduced number of experimental tests. However, the NIEL must be computed. Besides, even though the JPL method is a robust technique for degradation estimation, hundred of experiments for IV measurements in several cells are required to reduce the error. Furthermore, the degradation caused by radiation of electrons and protons at several energy levels and fluences and for each parameter of interest, *e.g.*, maximum power, should be measured.

The JPL method computes "critical fluences" normal to the cell surface at which each parameter gets an EOL value equal to 75% of its BOL. The RDCs for protons are computed by dividing the critical fluence corresponding to 10 [MeV] energy by the critical fluence at another energy level. The RDCs for electrons are similar but proportional to the critical fluence at 1 [MeV] energy. Then, the total number of incident particles is divided by two, as long as the rear surface of the cell is fully shielded, to compute the RDCs for omnidirectional particles.[2] Thus, the total equivalent normal fluence of 1 [MeV] electrons on bare PV-cells is

$$\phi_1\ \text{[MeV] electron, electrons} = \int \frac{d\phi_e(E)}{dE} R_e(E) dE, \tag{21}$$

$$\phi_1\ \text{[MeV] electron, protons} = D_{pe} \int \frac{d\phi_p(E)}{dE} R_p(E) dE, \tag{22}$$

$$\phi_1\ \text{[MeV] electron, TOT} = \phi_1\ \text{[MeV] electron, electrons} + \phi_1\ \text{[MeV] electron, protons}, \tag{23}$$

where D_{pe} is the "proton to electron damage equivalency ratio", which converts the equivalent fluence of 10 [MeV] protons to an equivalent fluence of 1 [MeV] electrons (~ 3000 for all parameters in Si-based PV-cells, but different in each parameter for GaAs-based PV-cells). Finally, the total damage is determined by comparing the equivalent total fluence with the characteristic degradation curve of the cell.

The NRL method requires the initial computation of the NIEL for electrons and protons. Then, the DDD due to protons is estimated by

$$D_{ddd,p} = \phi_p(E) S_p(E), \tag{24}$$

$$D_{ddd,p} = \int \frac{d\phi_p(E)}{dE} S_p(E) dE, \tag{25}$$

given that there exists a linear relationship between the RDCs of protons and the NIEL. On the other hand, the DDD due to electrons, where there is not a linear dependency with the NIEL, is given as

$$D^{eff}_{ddd,e}(1) = D_{ddd,e}(E) \left[\frac{S_e(E)}{S_e(1)}\right]^{n-1}, \tag{26}$$

$$D^{eff}_{ddd,e}(1) = \frac{1}{S_e(1)^{n-1}} \int \frac{d\phi_e(E)}{dE} S_e(E)^n dE. \tag{27}$$

where $D^{eff}_{ddd,e}(1)$ is the effective DDD due to 1 [MeV] electrons ($n = 1.7$ for GaAs PV-cells). Thereby, two characteristic curves are computed, one for degradation caused by protons and the other caused by electrons, which are aggregated into a single equivalent characteristic by

$$D_{tot} = D_{ddd,p} + \frac{D^{eff}_{ddd,e}(1)}{R_{ep}}, \tag{28}$$

representing the total dose at which the PV-cell is subjected. A drawback is that this method is still inaccurate for Si-based cells since its layers are too thick and the particle spectrum should be accurate-enough in the whole active region for this method.

Still during 2001, the radiation hardness of Si-, GaAs-, and GaInP-based PV-cells to the radiation of electrons was studied in [48]. The assessment was done by monitoring the short-circuit current and open-circuit voltage, which were proposed to be expressed by the following

$$I_{sc} = q\Phi_0 \left[1 - \frac{\exp(-\alpha W)}{1 + \alpha L}\right], \tag{29}$$

$$V_{oc} = \left(\frac{kT}{q}\right) \ln\left(\frac{I_{sc}}{I_0} + 1\right), \tag{30}$$

$$I_0 = \frac{q n_i^2}{N_R} \sqrt{\frac{D}{\tau}}. \tag{31}$$

For the radiation effect, the inclusion of compensating centers was considered by using (6). Besides, the minority-carrier lifetime was given in terms of the initial and after-radiation lifetime as

$$\frac{1}{\tau} = \frac{1}{\tau_0} + \frac{1}{\tau_i}, \rightarrow \frac{1}{\tau_i} = N_R \sigma_i \upsilon = K_R \phi, \tag{32}$$

where $N_R \propto \phi$, see Table 4.

[2] The effect of the coverglass upon the particle spectrum can be estimated by the range-energy tables and the "continuous slowing-down" method.

Table 4
Summary of the main remarks given by different studies.

Type of Cell and Remark	Ref.
Si	
Updating the mobility, due to the added deep-level traps, might improve the degradation modeling (suggested).	[12]
Protons produce deeper defects than electrons.	[12]
Increase of the SRV with the protons fluence.	[18]
The maximum conversion efficiency follows (1) inverse correlation between the base carrier concentration and the fluence lower than a threshold and (2) direct correlation between the base carrier concentration and higher fluences.	[29]
The anomalous degradation appears only when the diffusion length is comparable to the base thickness (theoretical explanation).	[15]
An adjusted NIEL is presented to overcome the issue of the NRL method to estimate the degradation of Si-based PV-cells.	[49]
GaAs	
A beam of mono-energetic, mono-directional protons between 1–10 [MeV] in unshielded PV-cells is representative of a space environment.	[25]
The largest damage is caused by the action of protons, followed by the neutrons, and finally the electrons.	[28]
The remaining efficiency (due to electron or proton bombarding) is much higher in the PV-cells with shallow junction in comparison with the cells with deep junction.	[4,7]
The degradation due to protons is mostly due to the induced electron traps.	[34]
Thinner the BSF, lesser the efficiency degradation.	[34]
The slope presented in radiated PV-cells resembling a typical shunt resistance is due to the voltage dependency of the photo-generated current.	[5,7]
Thin and highly-doped architectures might result in an end of life (EOL) power of higher than 90% of the beginning of life (BOL) value.	[6]
The use of multiple BRs allows to thin the cell while increase the radiation tolerance, accordingly.	[27]
The optical properties of a BR comprised of 20 periods made of AlAs/$Al_{0.1}Ga_{0.9}As$ are not affected significantly by a radiation fluence from 2×10^{14} to 1×10^{15} [e/cm^2] of 1 [MeV] electrons.	[36]
GaInP	
This PV-cell is harder to the radiation of electrons than Si-based and GaAs-based PV-cells, while Si-based is the weakest (especially for low fluences).	[48]
GaAs, GaInP	
Higher the electronic bonding structure directionality, more inaccurate the SRIM simulation.	[57]
The observed phonon intensity increments after radiation are due to changes in optical parameters.	[57]
GaInP/GaAs/Ge	
The GaAs layer is the main responsible for the degradation due to bombarding of electrons and protons.	[11,19,23,30,50]
The top layer degradation is mainly due to the damage to its emitter and to the interface among the top and middle layer given the increase of the recombination velocity.	[11]
The relative damage coefficient (RDC) for the open-circuit voltage reaches maximum values for proton ranges corresponding to the pn junctions.	[50]
The combination of the BR and the upper tunnel diode reduces the optical losses by parasitically absorption in the tunnel diode.	[54]
$InGaP_2$/GaAs/Ge	
The spectrum of omnidirectional 0.03–5 [MeV] protons produces a more uniform damage distribution across the cell when a coverglass (SiO_2) of 3 mils is used[1].	[8]
1–10 [MeV] protons are the most adequate for ground-based tests.	[8]
A beam of mono-energetic, normal incident, and low-enough energy protons to get trap inside the layers is not proper to characterize the actual cell behavior in a space environment.	[8]
A beam of high-enough energetic protons that traverse the active layers is adequate to characterize the actual cell behavior in a space environment.	[8]
The GaAs layer is the main responsible for the degradation due to bombarding of protons.	[8]
(LM) $Ga_{0.51}In_{0.49}P$/GaAs/Ge	
Lower the temperature, larger the degradation of the bottom cell for a specific fluence until becoming the current-limiting layer.	[16]
Increase of the reverse saturation current after radiation at very low temperatures is not observed.	[16]
The bottom layer presents the highest recovery after annealing.	[16]
(LM) GaInP/GaAs/Ge, (UMM) InGaP/InGaAs/Ge	
The power degradation in the UMM PV-cell is higher for 50 keV protons than for 150 keV, whereas the power degradation in the LM PV-cell is higher for the 150 keV protons than for 50 keV protons.	[21]
Low-energy protons reduce faster the shunt-resistance than the other parameters of a PV-cell.	[21]
(UMM) $Ga_{0.43}In_{0.57}P/Ga_{0.92}In_{0.08}As$/Ge, (LM)$Ga_{0.51}In_{0.49}P/Ga_{0.99}In_{0.01}As$/Ge	
The UMM cell presents similar degradation to the LM cell for protons bombarding.	[13]
(MM) $Ga_{0.44}In_{0.56}P/Ga_{0.92}In_{0.08}As$/Ge	
The use of the buffer layer like a BR along with more groups of layers to form a multi-BR increases considerably the whole efficiency showing a low sensitivity to the angle of incidence and higher radiation tolerance (for the case of light splitting).	[55]

(*continued on next page*)

Table 4 (*continued*).

Type of Cell and Remark	Ref.
$GaInP_2$/InGaAs/Ge	
The radiation by highly energetic protons degrades the shunt resistance.	[56]
The radiation by highly energetic protons does not contribute significantly to the deep-level defects concentration.	[56]
The traps in the interfaces increase non-linearly with the radiation of protons.	[56]
(LM) GaInP/GaInAs/Ge	
A BSF made of $Ga_{0.502}In_{0.498}P$, instead of AlGaAs, in the middle layer increases the radiation resistance.	[33]
The GaInAs layer is the main responsible for the degradation due to bombarding of electrons.	[33]
The light splitting by means of BRs allows to increase the efficiency of the cell by using external PV-cells while increasing the radiation tolerance by thinning subcells.	[53]
GaInP/$Ga_{0.99}In_{0.01}As$/Ge	
A double BR along with thickness optimization of subcells can improve the efficiency up to 5% at a rated radiation, but a lower BOL efficiency in comparison to cells without BR.	[52]
(IMM) InGaP/GaAs/InGaAs	
The radiation hardness of middle and bottom layers is improved by adding i-layers between the pn junctions.	[32]
(LM) GaInAsP/InP	
Higher the InP fraction, better the cell recovery after the annealing treatment.	[22]
Higher performance of a GaAs-based cell after radiation whereas lower performance after the annealing.	[22]
Ge	
Longer EOL diffusion length by reducing the doping concentration.	[10]
Radiation of electrons and protons increases the SRV.	[10]
InGaP/GaAs	
The GaAs layer is the main responsible for the degradation due to bombarding of electrons.	[24]
The annealing process is improved by illumination and forward current injections, even at RT.	[24]
GaInP/GaAs/$Ga_{0.7}In_{0.3}As$/$Ga_{0.42}In_{0.58}As$	
The subcell $Ga_{0.7}In_{0.3}As$ is the main responsible for the degradation due to electron bombarding.	[31]
The radiation resistance is improved by adjusting the thickness of the layers.	[31]
Any	
Particles with an energy range of 1–8 [MeV] upon uncovered cells are suitable to represent an actual space environment.	[9]

Note 1: Typically used in a geosynchronous earth orbit (GSO) (3 to 6 [mils]). In a HEO, the coverglass is typically larger than 6 [mils] and up to 30 [mils].

Later in 2002, due to the difficulty of measuring each layer individually in MJ PV-cells, authors in [30] proposed to use EL to study the degradation of a TJ PV-cell caused by bombarding of 1 [MeV] electrons. The EL intensity, which is related to the QE, depends on the amount of the non-radiative recombination centers, which depends on the amount and energy of the particles radiating the cell. Therefore, the QE was expressed as

$$\eta = \left(1 + \frac{\tau_r}{\tau_{nr}}\right)^{-1}, \tag{33}$$

$$\tau_{nr} = \left(\sigma \upsilon N_R\right)^{-1}, \tag{34}$$

$$N_R = K_R \phi. \tag{35}$$

where the luminescence intensity varies similar to QE with $\left(1 + \alpha_r \phi\right)^{-1}$, $\alpha_r = \tau_r \sigma \upsilon K_R$ (see Table 4). It was suggested to consider the hardest material (to radiation) to build the current-limiting layer.

In 2003, the issue identified in [9] was addressed in [49]. The NRL method failed to model the degradation of Si-based PV-cells due to the bombarding of nuclei particles. The problem lies in the assumption of the method that the energy of particles is considered constant across the layers while the Si wafers are too thick due to the low absorption coefficient. Thus, such an assumption is not accurate any longer in Si-based PV-cells, except for very high energetic particles. In this regard, this study proposed to use an adjusted NIEL to get the DDD caused by low-energy protons in Si. The adjusted NIEL is computed by dividing the total deposited energy in the material by its active region width. According to the SRIM software, protons with energies lower than 3 [MeV] are stopped inside the active region. The analytical values obtained for RDCs were close to the experimental results.

During the same year, another strategy was devised to analyze the degradation of each layer in a TJ PV-cell due to the bombarding of protons [50]. The proposed technique used light bias to get the spectral response (SR) of each layer at the BOL and EOL for different fluences. The results coincide with the estimation of the proton ranges (by TRIM) showing the major damage in the layer where the particles are stopped. Besides, the RDCs suggested by the JPL method were used (see Table 4).

Later in 2006, authors in [51] studied the GaAs PV-cell degradation of different brands under the bombarding of protons and electrons. The minority-carrier lifetime was given as

$$\frac{1}{\tau} = \frac{1}{\tau_0} + I_{ri} \sigma \upsilon \phi, \tag{36}$$

where I_{ri} was assumed proportional to the NIEL as $I_{ri} = \gamma S$ while γ (the proportional constant) was computed for 1 [MeV] electrons and kept constant from there forward. Initial minority-carrier recombination time was obtained by doing curve-fitting to the degradation curves of I_{sc} and V_{oc} vs fluence. Besides, information of IV-characteristics in darkness, deep-level transient spectroscopy (DLTS) combined with capacitance-voltage (C-V) measurements, I_{sc} and V_{oc} under illumination, and EL were used to obtain the initial value of $I_{ri}\sigma$ (1×10^{-12} and 1×10^{-13} [cm] for the *n*-type and *p*-type layers, respectively). The reported value for I_{ri} is 0.1 cm^{-1}. Then, these values were tuned for both n-type and p-type layers by doing curve-fitting to the degradation curves of I_{sc} and V_{oc}. The final (tuned) values reported for σ are $1{\times}10^{-11}$ and $1{\times}10^{-12}$ [cm^2] for an *n*-type and *p*-type layer, respectively. The parameter σ was considered constant and the final results were compared with the experimental data of 1 [MeV] for each sort of particle, showing a good agreement.

At that time, it was already known that an efficient technique to harden the MJ PV-cells is by narrowing the thickness of the hardest layer (to the radiation) to make it the current-limiting layer. However, the study of low energetic particles, which might be stopped inside such thin layers was limited. Therefore, the authors in [8] studied the effect of omnidirectional low energetic protons on the degradation of TJ PV-cells by analyzing three study cases: (1) Mono-energetic and unidirectional low-energy protons normally incident upon an uncovered PV-cell, (2) Mono-energetic and omnidirectional low-energy

protons incident upon an uncovered PV-cell, and (3) Omnidirectional spectrum.[3] of low-energy protons simulated to travel across a glass cover (space conditions). Besides, the impact of different coverglass thicknesses was studied.

The NIEL was estimated analytically and the slowed-down spectrum was computed by the continuous slowing-down approximation. The results showed a very severe degradation of the cell's maximum power for protons with energies between 250 and 380 keV, since the Bragg peak was located inside the GaAs (middle layer). Besides, a more uniform distribution of damage along the three layers for the study case (2) was obtained in comparison with the study case (1). Furthermore, it was shown that the more directional the spectrum, the higher the uniformity of damage across the PV-cell. Regarding the coverglass thickness, it was shown that 10 [μm] of SiO_2 was enough to preserve uniformity of degradation across the cell.

It was shown that under mono-energetic, normal incident, and low-enough energy protons to get trapped inside the layers, the damage distribution increases with the cell depth, unlike the omnidirectional spectrum (space conditions), that decreases with the depth (almost uniform inside the cell), see Table 4.

In 2008, authors in [11] studied the degradation of a similar TJ PV-cell caused by bombarding of low-energy protons. It was found that protons with energies lower than 1 [MeV] can degrade drastically the PV-cell performance. Besides, the results showed that the degradation is worsened with the fluence of particles or by decreasing the energy of the particles.

Another study in 2009 proposed a methodology to compute the carrier removal rate (R_c) and damage coefficient for the minority-carrier diffusion length (K_L) at different values of NIEL for different kinds of materials and particles [19]. The study was focused on TJ PV-cells that are radiated by protons and electrons with different energies and fluences. The model was built in the PC1D software consisting of three separate layers connected in series. Besides, it was assumed that the SRV increases with the fluence while the diffusion length (2) and carrier concentration (7) are reduced. The parameters R_c and K_L were determined through curve fitting using PC1D at different particle fluences for specific energies. It was shown that R_c increases by reducing the proton energies or increasing electron energies. The same tendency was reported for K_L, except for low energy levels. According to the study, R_c is linearly proportional to the NIEL, regardless of the particle type or target's material. While, K_L can be linearly (in case of protons, except for low-energy protons where saturation appears) or quadratically (in case of electrons) proportional to the NIEL. However, several significant differences between the simulation results and the actual EQE, especially for the longer wavelength regions, stressed the need for more investigation.

During the same year, the degradation process of a TJ PV-cell due to the bombarding of protons at different energies was studied in [20]. The degradation parameters R_c and K_L were computed by applying the curve-fitting technique to the EQE from PC1D software, where the model was comprised of three independent layers connected in series. In addition, it was assumed that the SRV increases with increasing the proton fluence. The minority-carrier lifetime, which can be split into radiative and non-radiative in general, is specified in detail by including the band-to-band, Auger, SRH, and surface lifetimes terms, as following

$$\frac{1}{\tau_{eff}} = \frac{1}{\tau_B} + \frac{1}{\tau_{Aug}} + \frac{1}{\tau_{SRH}} + \frac{S_F + S_R}{2d}, \tag{37}$$

$$= B_{bb}p + C_{Aug}p^2 + \frac{1}{\tau_{SRH}} + \frac{S_F + S_R}{2d}, \tag{38}$$

where it was assumed that τ_{SRH} decreases with the fluence whereas S_F and S_R increase. The initial minority-carrier diffusion length was modeled as

$$L = \sqrt{D\tau_{eff}} \tag{39}$$

[3] Corresponding to a HEO.

while the minority-carrier diffusion length and concentration after radiation were approximated by (2) and (7), respectively. The paper showed that for very short diffusion lengths (*e.g.*, less than 40 nm for a fluence of 10^{14} in the InGaP layer), the model is unable to fit the experimental results. Therefore, it was suggested that (2) requires further investigation to overcome this limitation.

In 2010, a software called "SCREAM" was introduced to study the degradation mechanism caused by the striking of energetic particles. The software applies the NRL method [28]. Besides, the slowed-down spectrum was analytically computed employing the slab geometry considering the continuous slowing down approximation. Thus, it was assumed that particles follow a straight trajectory throughout the shielding (9). In addition, the software can deal with multi-layer shielding by either using the actual stack or using the equivalent SiO_2 thickness, which is usually too conservative according to the study. The equivalent SiO_2 thickness is computed by summing up the areal densities [g/cm^2] of each material and converting them to an equivalent thickness using the density. According to this study, the physical nature of the non-linear dependency of the damage coefficients with the NIEL was not totally understood at that time. Finally, a relation between the JPL and NRL methods was proposed. However, the software was also unable to accurately represent the degradation behavior for materials with long active regions, *e.g.*, Si.

Still in 2010, a study analyzed the use of a BR and its effects upon the PV parameters due to bombarding of 1 [MeV] electrons in a TJ PV-cell [52]. The paper proposed to optimize the middle layer (GaInAs) thickness to maximize radiation hardness while the top layer (GaInP) thickness is optimized to match the subcell photo-generated currents. The diffusion length degradation due to 1 [MeV] electrons was expressed basically by (2) while $K_L = K/D$, where K represents the material damage factor. On the other hand, the open-circuit voltage of the j-th subcell was given in terms of the recombination current and the diffusion length, accordingly, before and after the radiation as

$$V_{oc}^{(j)} = V_{oc,0}^{(j)} - \frac{2kT}{q}\ln\left(\frac{L_{n,0}^{(j)}L_{p,0}^{(j)}}{L_n^{(j)}L_p^{(j)}}\right) \tag{40}$$

$$V_{oc,0}^{(j)} = \frac{2kT}{q}\ln\left(\frac{I_{ph}^{(j)}}{I_{r,0}^{(j)}}\right),$$

$$I_{r,0}^{(j)} = \frac{kTn_i}{\phi'}\frac{\sqrt{D_{n,0}^{(j)}D_{p,0}^{(j)}}}{L_{n,0}^{(j)}L_{p,0}^{(j)}}$$

where the suffix 0 means before radiation. In this study, single and double BRs were implemented to increase the photo-generated current in the thinned GaInAs layer, showing improvements in the efficiency from 2% to 5% in comparison to cells without BR. Besides, a better radiation resistance was shown when a double BR is used. It should be noticed that the optimization was carried out for specific fluences (optimal fluence) showing a lower BOL efficiency when the optimal fluence is higher.

Fig. 7 provides an illustrative representation of the different PV-cell architectures studied by the articles reviewed in this paper for the period 2001 to 2010. The element of the cell under analysis and the kind of particle used for the respective study are indicated.

2.4. Studies from 2011 to 2020

Another study in 2011 studied the radiation hardness improvement of a TJ PV-cell (GaInP/GAInAs/Ge) by thinning the middle layer while including a built-in BR [35]. One single BR was comprised of twenty periods of $Al_{0.1}Ga_{0.9}As$/AlAs, effectively reflecting the light in the range of 800–900 [nm]. A second double BR was made of twenty periods of $Al_{0.2}Ga_{0.8}As$/AlAs and twenty periods of $Al_{0.1}Ga_{0.9}As$/AlAs, with an effective reflection in the range of 750–900 [nm], allowing to thin even more the subcell. The diffusion length here was also estimated by (2)

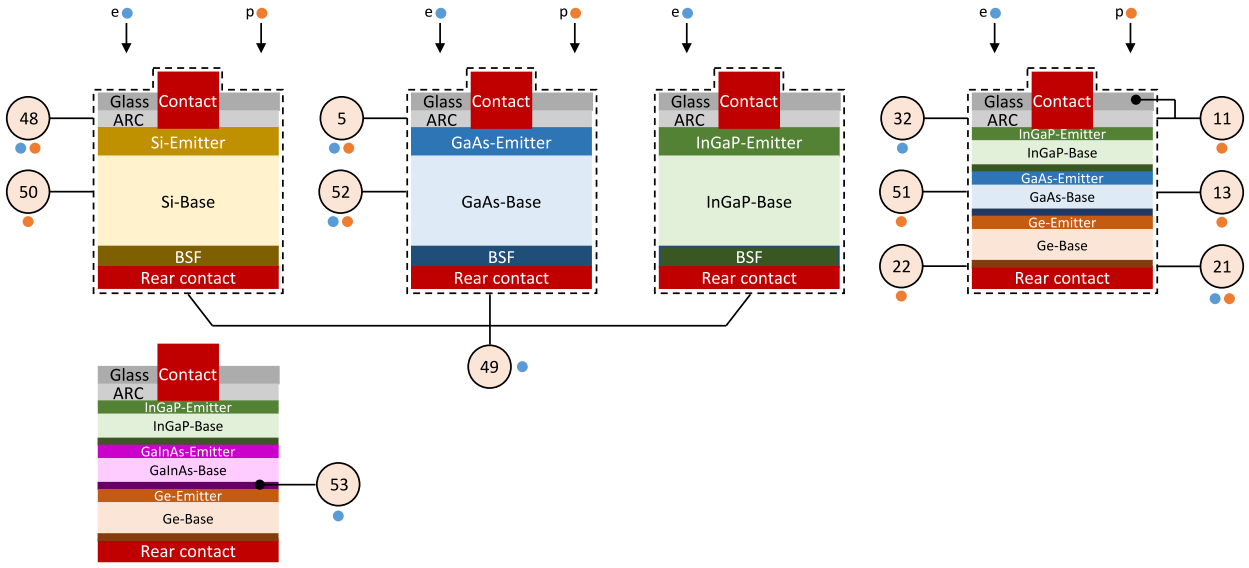

Fig. 7. Type of cells reviewed in this paper for the period 2001 to 2010. The labels indicate the element studied/optimized/compared in terms of radiation resistance by [8,9,11,19,20,30,47–52]. It should be noticed that the substrate may be present between the BSF and the rear contact. Note: The reader is referred to the reference list to see the exact concentration of each element of the compounds.

with $K_L = K/D$, where K is the material damage factor, and the open-circuit voltage was approximated by (40). According to the results, the double BR offers the best efficiency improvement (up to 2%) after a fluence of $3{\times}10^{15}$ [e/cm^2] with energy of 1 [MeV]. However, the authors claimed that the PV-cell efficiency is still limited by the middle subcell parameters, which are the fastest degrading ones. In this study, the whole cell was also optimized for a specific fluence, showing the higher the optimal fluence, the lower the efficiency at the BOL.

Later in 2012, a study proposed to split the light by means of a double BR, located in a LM GaInP/GaInAs/Ge PV-cell, to send the light with the wavelength in the range of 900–1050 [nm] to an external Si-based PV-cell [53]. Such an action might increase the radiation tolerance by optimizing the subcells thicknesses. The BRs were comprised of 15 periods of alternating GaAs/AlAs where the first reflector was centered at 940 [nm] and the second filter at 985 [nm] while ensuring an optimal current of the Ge subcell. According to the study, this configuration can increase the efficiency in the range of 2.5%–3.5% in comparison to the cell without the BR.

In 2014, authors in [32] proposed to build an IMM TF TJ PV-cell with a bottom layer of InGaAs instead of the traditional Ge or GaAs. The efficiency was increased up to 37.9% (at air mass 1.5 (AM1.5)) by reducing the series resistance, optimizing the ARC, optimizing the window, and increasing the bandgap of the bottom layer. The bandgaps from top to bottom layer were 1.88, 1.43, and 0.98 eV, respectively. Besides, the proposed TF PV-cell was 15 times lighter than the same cell architecture using a substrate of Ge, according to the authors. In addition, the radiation hardness of the middle and bottom layers was improved by adding i-layers between the pn junctions.

In the same period, [54] optimized a GaInP/GaAs/Ge PV-cell taking advantage of a distributed BR consisting of 16 periods made of $(Al_{0.1}Ga_{0.9})_{1-x}In_xAs$ and $Al_{0.8}Ga_{0.2}As$ to improve the radiation hardness against 1 [MeV] electrons. The Indium content was optimized to guarantee a lattice match between periods and the thickness of the middle layer was reduced. Besides, the optimization of the BR was in the range of 800 to 900 [nm] by means of the characteristic matrices method. The study proposed to combine the BR with the upper tunnel diode to prevent the parasitically absorption of the light reflected. The PV-cells having BRs were radiated with fluences from 3×10^{13} to 1×10^{16} [e/cm^2] and compared with PV-cells without BR. The results indicated an improved efficiency for more than 10% relative to the efficiency of the PV-cells without BR at the largest fluence and a higher EQE, especially for the longer wavelength region.

In 2018, the degradation hardness caused by the proton bombarding of similar TJ PV-cells, which were built by different processes (UMM and LM) was studied in [13]. According to the study, the efficiency of the LM cell might be increased by metamorphic configurations if the top and middle cell's bandgaps are reduced, or if the bottom cell's bandgap is increased to 1.0 eV by using $Ga_{0.7}In_{0.3}As$. However, in metamorphic configurations, there might exist larger lattice mismatches, which would produce dislocations and an efficiency drop, accordingly. Therefore, two approaches to build the PV-cells with layers of different lattice constant were highlighted: Monolithic and Non-Monolithic. In the non-monolithic approach, the layers are grown separately and then connected by different techniques. While in the monolithic approach, the layers are grown one after another and a buffer layer is incorporated between them to gradually release the strain produced by the mismatch of the lattice constants. The monolithic approach can be categorized by two approximations based on the fabrication method, namely IMM and UMM. According to the study, the UMM had reached efficiencies up to 31% under air mass zero (AM0) while being fully compatible with the LM fabrication technologies. Thus, a lower production cost compared to other strategies was implied. The results indicated that the UMM cell presented a lower strain among the top and middle layers, compared to the LM cell.

The study used the NRL method to analyze the degradation. Both structures showed similar parameters degradation (short-circuit current, open-circuit voltage, and maximum power) in two proton energy levels while observing a higher degradation for the lowest 3 [MeV] protons in both architectures. In this regard, it was suggested that by increasing the fractions of In and P in the compositions of the layers, the radiation hardness might be improved against the 3 [MeV] protons bombarding. In addition, the top layer of the UMM-cell presented a lower BOL EQE given the extra dislocations added by the difference in lattice constants. However, the UMM's top layer radiation hardness was shown to be stronger than the LM's respective layer while the middle layer hardness was weaker.

During the same period, the degradation of a LM TJ PV-cell due to 1 [MeV] protons was studied in [16] at low-intensity and low-temperature (LILT) conditions, which are common in interplanetary missions[4]. The study highlighted that the phenomena like defect annealing, junction behavior under stress, and tunneling are not observable at the RT and should be taken into account. The experimental

[4] A vacuum of 10^{-7} [mbar] was considered.

tests were performed by analyzing each layer individually in the same TJ configuration, while the other layers were acting like filters, *i.e.*, three cells were used to analyze one full TJ configuration. According to the results, the bottom cell became the current-limiting layer at the lowest temperatures while for the temperature of 200 and 300 K, the middle cell was the current-limiting layer, both for large fluences. The conclusion was that the bottom cell degradation at low temperatures is not caused by the minority-carrier recombination, but by the reduction of the effective cell area given that no increase of the reverse saturation current was observed after radiation that implies no new defects were added. It was proposed that each proton leaves a cylindrical charge path along its track. Thereby, the effective area after a fluence of radiation is

$$A_{ef} = A_0 - \phi A_0 \pi r^2, \tag{41}$$

$$1 - RF(I_{sc}) = 1 - \frac{A_{ef}}{A_0} = \phi \pi r^2, \tag{42}$$

where RF means "remaining factor". In general, a strong dependency on temperature was observed. Moreover, it was shown that the open-circuit voltage deduced from the three individual layers to the whole package was accurate whereas the short-circuit current accuracy was not enough. The annealing process was also applied at different temperatures (below 300 K).

In 2018, different parameters of several PV-cells, namely InGaP, GaAs, Ge, Si, and InGaP/GaAs/Ge were also assessed in [60] while cells were exposed to different temperatures under AM0 spectrum. The bandgap of the compound materials was approximated by

$$E_{gi}(A_{1-x}B_x) = (1-x)E_g(A) + xE_g(A) + xE_g(B) - x(1-x)P. \tag{43}$$

The results indicated a better performance for the TJ PV-cell.

Another study was published in 2018 in [5]. In which, the voltage dependency of the photo-generated current at RT of GaAs PV-cells was shown when cells are exposed to different electron and proton fluences considering diffusion length shortening for the degradation process. The study suggested that such a voltage dependency stems from the depletion region width shortening by the application of forward bias and is responsible for the slope of the IV characteristics after radiation, resembling the typical shunt resistance. Their suggestion was based on the fact that the same phenomenon in the measured dark IV profiles was not observed. However, such a dependency should be important only when the summation of both diffusion lengths (for holes and electrons) and the depletion region width is smaller than the cell thickness, *e.g.*, in heavily irradiated cells. The photo-generated current was computed by

$$I_{ph} = I_{ph,p} + I_{ph,n} + I_{ph,W}, \tag{44}$$

where $I_{ph,p}$, $I_{ph,n}$, and $I_{ph,W}$ are related to the holes in the quasi-neutral region (QNR) of n-layer, electrons in the QNR of p-layer, and electron–holes in the depletion region, respectively. Each term of (44) was computed by integrating the generation rate at a distance x from the surface, $\alpha\Phi_0 \exp(-\alpha x)$, with a probability for collecting electron–hole pairs. The final expression for I_{ph} was given as

$$I_{ph} = e\Phi_0 \left[\frac{\alpha L_p}{\alpha L_p - 1} \left(e^{-x_1/L_p} - e^{-\alpha x_1} \right) + e^{-\alpha x_1} \left(1 - \frac{e^{-\alpha W}}{1 + \alpha L_n} \right) \right], \tag{45}$$

while W was expressed by (10). The absorption coefficient α was assumed constant (the average value between 650 and 900 [nm]) and the SRVs were neglected. Besides, Φ_0 was being adjusted in (45) until I_{ph} reached the short-circuit current of a non-radiated cell.

The results showed a good agreement among the experimental and simulated IV-characteristics. Besides, it was stated that the diffusion length depends only on the DDD and not particles type nor energy as

$$\frac{1}{L_\phi^2} = \frac{1}{L_0^2} + K_L D_{ddd}, \tag{46}$$

Afterwards in 2019, a study was dedicated to comparing the degradation of an UMM and a LM TJ PV-cell due to the bombarding of low energetic protons [21]. In this study, it was assumed that the top layer is thick-enough to bring the particles to the rest. The results related to the UMM PV-cell indicated that the 50 keV protons caused a higher degradation in the shorter-wavelength region (top layer) and the short-circuit current, accordingly. On the other hand, the longer-wavelength region was more degraded by the 150 keV protons, which represented a higher degradation of the open-circuit voltage. Besides, comparing both technologies, the results indicated a slightly higher power degradation of the UMM-cell. However, the open-circuit voltage was much more degraded in the LM PV-cell, especially for 150 keV protons, given that these particles traverse the top layer introducing more defects in the depletion region. In addition, they also reported the presence of *artifacts*[5] in the UMM after the proton radiation. Finally, it was concluded that the proton radiation caused an increase of the dark saturation current and a decrease of the shunt resistance.

In the same year, thin GaAs-based PV-cells were studied in terms of geometry to find a balance between the specific power (W/kg) and the radiation robustness [6]. In this respect, the shallow and deep junction configurations with a back reflector were assessed with the base of p-type and n-type. Besides, the effect of the base thickness and doping concentration was studied. The SRVs were assumed constant while the diffusion length degradation and the carrier compensation were expressed by (2) and (6), respectively. According to the results, two thin and highly-doped cells are good candidates for space applications. Namely, the traditional shallow junction p-type base and a deep junction n-type base, both having an EOL maximum power of higher than 90%. Finally, it was stated that the degradation levels for highly-doped and ultra-thin configurations with a lower BOL power density are smaller than 3%. However, the study had not taken into account several phenomena for highly doped materials, such as the Moss-Burstein effect, Auger recombination, or the effects caused by the electrically inactive dopant incorporation.

Still in 2019, several distributed BRs were implemented in a LM $Ga_{0.51}In_{0.49}P/Ga_{0.99}In_{0.01}As/Ge$ and in a metamorphic (MM) $Ga_{0.44}In_{0.56}P/Ga_{0.92}In_{0.08}As/Ge$ TJ PV-cell for light splitting [55]. The spectrum band reflected optimally was in the range of 900–1050 [nm] and sent to an external Si-based cell. For the LM cell, four versions of a BR were implemented: 1- The BR was made of 16 periods of $Al_{0.2}Ga_{0.8}As/Al_{0.8}Ga_{0.2}As$. 2- A multiple BR comprised of two groups with eight periods each and different period thickness in both groups. 3- A multiple BR with two groups and 16 periods each and again different period thickness in each group. 4- A multiple BR with three groups and 16 periods each and again different period thickness in each group. According to the results, the highest efficiency was provided by version 4. On the other hand, for the MM cell, the buffer was utilized also as the BR. For this case, four versions were implemented: 5- Eight periods of GaInAs/GaInP, where the concentration of In in the GaInAs of each period was progressively increased from 1% to 8% (from bottom to top). 6- Eight periods of GaInP/GaInAs/GaInP with concentrations that ensure matching of lattice constant and different refractive indices. 7- Version 6 was complemented with another group of 16 periods made of $Ga_{0.44}In_{0.56}P/Ga_{0.92}In_{0.08}As$. 8- Version 6 was complemented with two groups of 16 periods each and made of $Ga_{0.44}In_{0.56}P/Ga_{0.92}In_{0.08}As$. According to the results, the best efficiency was achieved from version 8. Besides, the BR showed a very low sensitivity to the angle of incidence. Regarding the modeling, the WVASE software was used to adjust the computed reflectance with the measured data by means of the subcells thickness adjustment.

Another work in 2019 explored how the current density reduced by thinning a GaAs-based PV-cell can be recovered by including a BR while the radiation tolerance is increased [36]. The BR was comprised

[5] It consists of an EQE increment in the longer wavelength region.

of 20 periods made of AlAs/$Al_{0.1}Ga_{0.9}As$. And the radiation consisted of fluences from 2×10^{14} to 1×10^{15} [e/cm^2] of electrons having energies of 1 [MeV]. According to the results presented, for such a range of fluences, the effective spectrum band reflected by the BR is not significantly affected (nor the magnitude, neither the location of peak value) and it is considered constant along the fluences, accordingly. Besides, taking into account the results of the SJ GaAs cell, the study suggested a possible improvement of 0.24% absolute efficiency in a $InGaP_2$/GaAs/Ge radiated by 1×10^{15} [e/cm^2] electrons having energies of 1 [MeV] when the middle layer is half and a BR is implemented.

Recently in 2020, authors in [4] analyzed the effect of the junction depth upon the degradation of GaAs PV-cells due to the 1 [MeV] electron bombarding. Besides, the layer thickness effect was analyzed using TF and substrate-based PV-cells. The carrier transportation in the quasi-neutral regions was modeled using diffusion current equations while considering a negligible electric field and constant material parameters. Thus, the total photo-generated current was computed by the summation of the respective currents generated in the quasi-neutral regions and depletion region. The efficiency for collecting carriers in the depletion region was assumed unitary. The current density was obtained by calculating the integration of the spectral photon flux weighted by its respective EQE over the wavelength. The expressions can be

$$\eta_{EQE,\lambda} = \frac{\#\text{ carriers}}{\#\text{ photons}} = \frac{nh\nu}{mh\nu} = \frac{nhc}{\lambda E_\lambda}\frac{q/\Delta t}{q/\Delta t} = \frac{hc}{q\lambda}\left(\frac{nq/\Delta t}{E_\lambda/\Delta t}\right) = \frac{hc}{q\lambda}\left(\frac{I_\lambda}{P_\lambda}\right) = \frac{hc}{q\lambda}\text{S.R.}, \tag{47}$$

$$J = q\int_{\lambda_i}^{\lambda_f} \eta_{EQE,\lambda} F_\lambda d\lambda. \tag{48}$$

Besides, the optical reflectance in the window-emitter and base-BSF interfaces were computed by electromagnetic simulations in 1D. The minority-carrier lifetime considering the radiative and non-radiative recombination lifetime is

$$\frac{1}{\tau} = \frac{1-f_{PR}}{\tau_r} + \frac{1}{\tau_{SRH}}, \tag{49}$$

where the radiative lifetime is $\tau_r = 1/R_{RAD}N_x$ and "x" can refer to "a" of acceptors or "d" of donors. The reverse saturation current density is written in terms of the current provided by the emitter and the base, such as

$$J_0 = J_{01}\left[\exp\left(\frac{qV}{kT}\right)-1\right] + J_{02}\left[\exp\left(\frac{qV}{2kT}\right)-1\right], \tag{50}$$

$$J_{01} = J_{01,Emitter} + J_{01,Base}, \tag{51}$$

$$J_{01,Emitter} = \frac{qD_p n_{i,E}^2}{L_p N_d}\left[\frac{\sinh\left(\frac{d_E}{L_p}\right) + \frac{S_p L_p}{D_p}\cosh\left(\frac{d_E}{L_p}\right)}{\cosh\left(\frac{d_E}{L_p}\right) + \frac{S_p L_p}{D_p}\sinh\left(\frac{d_E}{L_p}\right)}\right], \tag{52}$$

$$J_{01,Base} = \frac{qD_n n_{i,B}^2}{L_n N_a}\left[\frac{\sinh\left(\frac{d_B}{L_n}\right) + \frac{S_n L_n}{D_n}\cosh\left(\frac{d_B}{L_n}\right)}{\cosh\left(\frac{d_B}{L_n}\right) + \frac{S_n L_n}{D_n}\sinh\left(\frac{d_B}{L_n}\right)}\right]. \tag{53}$$

For calculating J_{02}, non-radiative recombination mechanisms in the depletion region were considered, which were modeled by the SRH theory taking into account multiple trap levels. Besides, the narrowing effect was considered for the highly-doped regions as

$$\Delta E_g \approx 2\times10^{-11}N_a^{1/2}, \quad \rightarrow \quad p\text{-type GaAs}, \tag{54}$$

$$\Delta E_g \approx 2\times10^{-8}N_d^{1/3}, \quad \rightarrow \quad n\text{-type GaAs}. \tag{55}$$

Under the condition $L_p \ll d_E$ and $L_n \ll d_B$ (thick quasi-neutral regions), the expressions from (51) to (53) approximate to the classical Shockley equation for the dark saturation current density as

$$J_{01} = J_{01,Emitter} + J_{01,Base} = \frac{qD_p n_{i,E}^2}{L_p N_d} + \frac{qD_n n_{i,B}^2}{L_n N_a}. \tag{56}$$

On the other hand, the expressions for thin quasi-neutral regions, $L_p \gg d_E$ and $L_n \gg d_B$, are reduced to

$$J_{01} = J_{01,Emitter} + J_{01,Base} = \frac{qD_p n_{i,E}^2}{N_d}\frac{S_p}{D_p + S_p d_E} + \frac{qD_n n_{i,B}^2}{N_a}\frac{S_n}{D_n + S_n d_B}. \tag{57}$$

The model contains four tuning parameters including S_p, S_n, τ_p, and τ_n, where τ_p and τ_n were expressed by (49). The degradation effect was modeled by (32) for the minority-carriers lifetime while the radiative term at the BOL was neglected. In addition, the SRVs in the interfaces window-emitter and base-BSF were proposed to be

$$S_p = S_{p,BOL} + K_p\phi, \tag{58}$$

$$S_n = S_{n,BOL} + K_n\phi, \tag{59}$$

where the damage coefficients for the SRVs were obtained by curve fitting.

The model results had a good accuracy compared with the experimental data. However, there were still differences, especially for the TF technology. In general, the study concluded that TF cells with back reflectors and shallow junctions are the best option for space applications.

Until 2020, the InP-based PV-cells had proven a stronger radiation hardness than those based on GaAs and it was believed that this property was related to the InP fraction in the material. Therefore, in [22], this assumption was studied by using a LM GaInAsP/InP PV-cell for different InP fractions (defined as the percentage of either In or P, whichever is the lowest), which produced different bandgaps. For instance, 0.9 eV for $Ga_{0.31}In_{0.69}As_{0.67}P_{0.33}$, 1.0 eV for $Ga_{0.23}In_{0.77}As_{0.49}P_{0.51}$, and 1.1 eV for $Ga_{0.16}In_{0.84}As_{0.34}P_{0.66}$. No considerable performance difference at the BOL for different compositions was reported. Besides, the annealing process (several days of annealing at open-circuit conditions) was studied with the typical conditions of a GEO, 60 [°C], and AM0. The doping concentration was estimated using electrochemical capacitance-voltage (ECV) measurements. The composition was estimated by the lattice constant, which was measured using X-ray diffraction and the bandgap, which in turn was computed by EQE measurements.

The minority-carrier recombination was modeled by considering the radiative and non-radiative (SRH and Auger) recombinations. The SRV at the interfaces was also considered. In addition, the study assumed that radiation was only affecting the non-radiative recombination time, while all the other parameters were considered not to be affected by radiation. Accordingly, only the non-radiative SRH lifetime was considered for curve fitting. The minority-carrier lifetime was expressed by

$$\frac{1}{\tau} = \frac{1}{\tau_{r,0}} + \frac{1}{\tau_{nr,0}} + \frac{1}{\tau_{id}}, \tag{60}$$

where the lower-script "0" indicates at the BOL and τ_{id} is zero before radiation. Thereby, τ_{id} was expressed as

$$\frac{1}{\tau_{id}} = \left(\frac{1}{\tau} - \frac{1}{\tau_0}\right) = k_R\phi. \tag{61}$$

This study used the irradiation-induced defect recombination coefficient, k_R, to assess the radiation hardness of the cells. Besides, k_R was considered to be independent of the BOL material quality, the cell structure, or the radiation dose while it was considered to be a constant value depending on the material and doping polarity.

The results indicated a large open-circuit voltage decrease caused by a relatively low fluence of electrons due to the high minority-carrier lifetime in the GaInAsP at the BOL. Besides, a considerable degradation at the longer wavelength region was shown. In addition, it was proven that the higher the InP fraction, the better the cell recovery after annealing treatment. The experimental and theoretical results showed good-enough agreement in terms of open-circuit voltage and internal

quantum efficiency (IQE). Moreover, the study compared the GaInAsP cell with another cell based on GaAs. The results showed a higher performance of the GaAs after radiation, but a lower performance after the annealing. Finally, it was concluded that the energy levels of the defects and their capture cross-sections change with the InP fraction.

Authors in [23] studied the open-circuit voltage degradation of individual subcells in a TJ PV-cell due to 1 [MeV] electrons bombarding by using EL measurements. In this respect, the reciprocity equation between the PV-cell and light emitting diode was used as follows

$$\varphi_{EL} = \eta_{EQE}(E) F_{bb}(E) \left[\exp\left(\frac{V}{V_T} \right) - 1 \right]. \tag{62}$$

The open-circuit voltage of each layer was computed by using the Boltzmann approximation for the photon flux of the black body F_{bb} to estimate the relative EL degradation of intensity as

$$\Delta\varphi_{EL} = \exp\left(\frac{\Delta V_{oc}}{V_T} \right), \tag{63}$$

where $\Delta\varphi_{EL}$ is the ratio between the EL intensity after and before the radiation. Then, the relative EL degradation of intensity was equated to the relative QE degradation, which is the ratio between QE after and before the radiation (QE at BOL is assumed unitary), as

$$\Delta\varphi_{EL} = \frac{\eta_{EQE}}{\eta_{EQE,0}} = \left[1 + \left(\tau_r I_{ri} \sigma_i \upsilon \right) \phi \right]^{-1}. \tag{64}$$

Thereby, the open-circuit voltage degradation (per layer) after radiation, by using (63) and (64), is

$$\Delta V_{oc} = V_T \ln\left[1 + \left(\tau_r I_{ri} \sigma_i \upsilon \right) \phi \right]^{-1}. \tag{65}$$

Eq. (65) was fitted to an experimental curve to compute the capture cross-section of non-radiative recombination centers, σ. The results showed that GaAs (middle layer) was the layer with the largest open-circuit voltage degradation, followed by the Ge-based layer (bottom layer), and finally the GaInP-based layer (top layer). Besides, a good-enough accuracy of the model compared with the experimental data (open-circuit voltage degradation) was reported. Where the lowest accuracy was related to the top layer (GaInP).

Another work reported in 2020 studied the degradation behavior of a LM DJ PV-cell caused by the bombarding of electrons and protons [14]. The study applied the NRL method to estimate the degradation, where the NIEL was computed as

$$S(E) = n_a \cdot \int_{T_d}^{Q_{max}} \left. \frac{d\sigma_{niel}}{dQ} \right|_E (Q) \cdot G(Q) \cdot Q \cdot dQ. \tag{66}$$

Besides, the short-circuit current density was given as

$$J_{sc} = \int_{\lambda} SR(\lambda) \cdot S_{AM0}(\lambda) d\lambda, \tag{67}$$

$$= \int_{\lambda} \frac{q\lambda}{hc} \eta_{EQE} \cdot S_{AM0}(\lambda) d\lambda, \tag{68}$$

where the spectral response at a specific wavelength $SR(\lambda)$ is obtained from (47). Then, the DJ cell was compared with some SJ PV-cells in terms of the remaining factor of maximum power. The DJ showed a poorer radiation hardness than most of the other cells highlighting that the main reason is severe degradation of I_{sc} and V_{oc} in both layers of the DJ cell due to its architecture. Additionally, the results showed that the 3 [MeV] protons were the most damaging particles. Moreover, a higher decrement of the EQE in the longer wavelength region was reported given that the likelihood of the photo-generated carriers being captured by the newly added defects (the deeper, the more defects) is much higher in the base of a shallow junction architecture. Finally, the top layer (InGaAsP) was always the current-limiting layer.

Authors in [56] studied the degradation of a TJ PV-cell caused by the radiation of 24.5 [MeV] protons. The protons were radiated at 170 [Gy] ($\sim 1.06\times10^{12}$ [[MeV]/g]). The carrier concentration was measured utilizing the C-V technique and the depletion capacitance was given as

$$C^{-2} = \frac{2\left(V_{bi} + V\right)}{qA_s^2 \epsilon\epsilon_0 N_d}, \tag{69}$$

which is used to estimate N_d. The depletion region width was expressed as

$$W = \sqrt{\frac{2\epsilon_s V_{bi}}{qN_d}}. \tag{70}$$

Moreover, the conductance-frequency (G-F) measures were used to compute the interface trap density as

$$D_{it} = \frac{2.5}{qA_s} \left(\frac{G_p}{w} \right)_{max}. \tag{71}$$

The interface trap density and trap time constant were derived from the peak conductance.

According to the results, V_{oc} was more degraded than I_{sc}. Hence, it was concluded that defects caused by proton radiation increase the reverse saturation current, and the open-circuit voltage decreases accordingly. Another reason given was the increase of defects in the depletion region by radiation, which would lead to a shunt-resistance reduction with a consequent reduction of the open-circuit voltage. This study also showed capacitance-frequency (C-F) measurements at zero bias (*i.e.*, no voltage applied). Besides, a very small difference of the capacitance (contribution to the total capacitance due to interface traps) was observed at different doses, suggesting no contribution to the deep-level defects concentration. Finally, it was concluded that the degradation caused by protons is more severe than degradation due to electrons given the higher collision density of the protons.

According to [10], a promising PV-cell candidate for space applications is the four-junction (FJ) metamorphic PV-cell with optimized current match, where the bottom cell is made of Ge. In this regard, this paper studied the Ge wafers degradation due to the bombarding of 1 [MeV] electrons and protons in more than 300 samples. Besides, the samples were subjected to an annealing process at 400 [°C] for 5 min and 30 min in one batch.

It was proposed to reduce the doping concentration while the minority-carrier lifetime (measured by microwave photo-conductance decay (μW-PCD) mappings) was increased using surface passivation with a Si_xC_{1-x} layer stack. However, the SiC layers were not only designed in a way to support the minority-carrier lifetime increment, but also to work as a mirror to photons ("mirror" layers) to increase the absorption in the longer wavelength region.

The experimentation was carried out by modifying different features of the "mirror" layers: the thickness, the doping concentration, and the annealing time. However, it was shown that none of these modifications affected or improved the degradation process at all. In addition, the doping and thickness of the Ge layer were also modified. The results indicated a longer EOL diffusion length by reducing the doping concentration whereas it was reduced with increasing the fluence of particles.

This study considered three kinds of minority-carrier lifetimes: effective, bulk, and surface, as follows

$$\frac{1}{\tau_{eff}} = \frac{1}{\tau_{bulk}} + \frac{1}{\tau_{surf}} = \frac{1}{\tau_{bulk}} + \frac{2}{W_{wafer}} S_{eff}, \tag{72}$$

which were plotted for different wafer thicknesses in the x-axis, $2/W_{wafer}$, and inverse effective lifetime in the y-axis, $1/\tau_{eff}$. Then, approximating to a linear function, S_{eff} represents the slope while the term $1/\tau_{bulk}$ represents the y-axis crossing. Thereby, the minority-carrier lifetimes were found for the bulk and surface. Besides, it was concluded that an important matter for the application of passivation for space PV-cells is to determine for which fluence the passivation is still effective to allow collecting all the current from the Ge layer. Finally, it was highlighted that lowly-doped and passivated Ge wafers

are very good candidates to be used as subcells in future space PV-cells in moderate radiated environments.

In [33], the effect of using a BSF made of $Ga_{0.502}In_{0.498}P$ instead of AlGaAs in the middle layer of a TJ PV-cell, GaInP/GaInAs/Ge, was studied focusing on the radiation-induced degradation caused by 1 [MeV] electrons. The study showed that the PV-cells with the middle layer's BSF made of GaInP have a higher radiation resistance. Besides, no significant difference among the cells' performance at the BOL was observed. Finally, the EQE pointed that the whole degradation is mostly due to the GaInAs layer.

The study of degradation of a FJ PV-cell GaInP/GaAs/$Ga_{0.7}In_{0.3}As$/$Ga_{0.42}In_{0.58}As$ (1.85 eV, 1.42 eV, 1.0 eV, and 0.7 eV) caused by electron radiation was made in [31]. Besides, the authors provided study of degradation of a SJ PV-cell made of the third sub-layer, which was proposed by them, caused by proton bombarding. The degradation analysis was carried out employing the NRL method. The same DDD for all the layers was assumed by considering similar trap densities and cross-sections. The short-circuit current was given by (29) while considering that the degradation stems exclusively from the decrease of the minority-carrier lifetime.

The results show some inaccuracies, especially near the MPP. Besides, the current of the second and third layers was increased while the current of the layer made of GaInP (the hardest layer to the radiation) was reduced at the BOL, resulting in improved radiation resistance. The DDD for a one-year mission on the GSO and also on LEO were presented in terms of the coverglass shielding thickness. The results for the GSO indicated that the largest damage is caused by the trapped electrons, followed by the solar protons, and the GCRs (which were tiny and neglected accordingly). The results for the LEO indicated that the largest damage is caused by the solar protons, followed by the trapped protons and trapped electrons. The GCRs contribution to the DDD was neglected.

Still in 2020, another study reported the application of a 13 periods BR, made of AlInP/InGaP and centered at 880 [nm], to a DJ LM InGaP/GaAs and a SJ GaAs PV-cells [37]. Apart from the BR, to further increase the remaining efficiency, multi quantum wells (MWQs) has been incorporated, showing improvements in the short-circuit current density of 2.84% and >9.8% for the SJ and bottom subcell of the DJ PV-cell, respectively, with respect to a corresponding baseline cell. According to the results, when the DJ cell is submitted to radiation of 1 [MeV] electrons at 1×10^{15} [e/cm^2], the cell with the MWQs+BR shows an improved remaining power of about 7% with respect to the baseline cell.

Fig. 8 provides an illustrative representation of the different PV-cell architectures studied by the articles reviewed in this paper for the period 2011 to 2020. The element of the cell under analysis and the kind of particle used for the respective study are indicated.

2.5. Studies in 2021

During the present year 2021, several studies related to the radiation-induced degradation of III–V PV-cells have been published. In [34], degradation of GaAs (p^+nn^+) PV-cells considering different kinds of defects caused by radiation of 1 [MeV] protons is studied. Simulations were carried out in the SCAPS software considering the presence of electron and hole traps, which had been identified by other studies (five electron traps and four proton traps). The analysis was conducted by considering effects of the hole and electron traps separately. Then, the results were compared with the case where all the traps (for holes and electrons) were considered. According to the results, the electron traps were the most important. Specifically, the two traps located almost at the intrinsic Fermi level, which are usually considered recombination centers, were the most damaging. Regarding the hole traps, just one trap (the deepest) showed the most important degradation contribution. The paper also studied the effect of the BSF thickness upon the degradation. The results showed a lower efficiency degradation by decreasing the thickness of the BSF.

Another work studied the damage distribution of undoped samples of GaAs and $In_{0.499}Ga_{0.501}P$ using photo-luminescence spectroscopy (PLS) and Raman spectroscopy (RS) due to the proton radiation [57]. Besides, the differences between the experimental and simulation results regarding the particle ranges were analyzed. The results indicated that SRIM overestimates the range of the protons in the InGaP. Such an error increased with the protons' energy. However, the results related to the GaAs compound had an excellent agreement with the experimental values. According to the authors, the reason for these different results lies in the fact that in GaAs the bonding structure distribution and the electronic charge density are much better represented by a homogeneous electronic charge density (similar to what is done in SRIM), compared to the case with the InGaP material.

The authors in [7] used the model introduced in [4] for studying the degradation of different GaAs PV-cell architectures (shallow and deep junctions, as well as substrate- and TF- based cells) due to proton bombarding. The degradation parameters corresponding to protons were computed using the degradation parameters related to electrons by employing the DDD approximation. The IV-characteristics were modeled based on the Hovel model including reflectances and photon recycling effects. The dark IV-characteristics were represented using two parallel diodes. The SRVs at the interfaces were expressed by (58) and the SRH minority-carrier lifetime was modeled by (32). Furthermore, the study considered a photo-generated current dependent on the voltage, which explained the effect of a reduced shunt resistance in the radiated IV-characteristics. In this respect, the depletion region widths, corresponding to the emitter and base, were given as

$$w_E = \sqrt{\frac{2\epsilon\epsilon_0}{q}\frac{N_a}{N_d\left(N_a+N_d\right)}\left(V_{bi}-V\right)}, \tag{73}$$

$$w_B = \sqrt{\frac{2\epsilon\epsilon_0}{q}\frac{N_d}{N_a\left(N_a+N_d\right)}\left(V_{bi}-V\right)}. \tag{74}$$

The results showed that simulated and experimental EQEs followed the same behavior for different fluences. Finally, the study highlighted that two architectures have the highest radiation hardness, namely substrate and TF-based cells with shallow junctions.

3. Discussion

Nowadays, the MJ PV-cells based on III–V compounds are the main source for the energy supply of many satellites and spacecrafts, even at extreme conditions (*e.g.*, LILT) to support ancillary services. However, this technology is still under study mainly towards lighter, more efficient, and more radiation-resistant PV-cells. The reason lies primarily in the launching costs and the hazardous environments that exist in outer space, especially for places far away or very close to the Sun, which might reduce considerably the lifetime of the PV-cells. In this respect, many studies have been carried out to understand the degradation mechanisms of PV-cells under such conditions. Table 4 provides a summary of the main remarks identified throughout the review process of important studies in this field from 1990s up to the present. Nevertheless, the readers are referred to the provided references to check out the very specific conditions at which such remarks apply.

Additionally, some challenges regarding the radiation-induced degradation that the PV technology, based on III–V semiconductors, still faces were identified and listed as follows:

1. Even though the GaAs-based PV-cells are among the most efficient ones, with a relatively cheap production cost, a relatively high efficiency, and part of most MJ architectures, the radiation resistance should still be under investigation. Many studies on MJ cells have proven that the layer based on GaAs is mainly

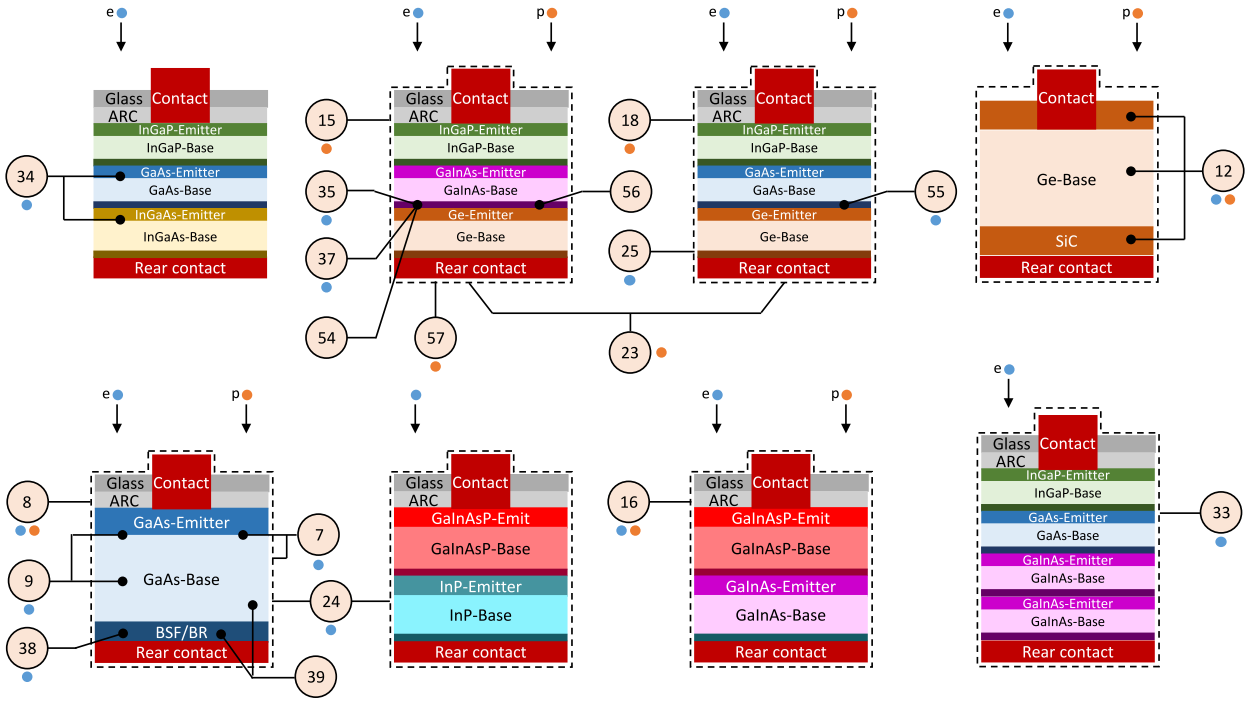

Fig. 8. Type of cells reviewed in this paper for the period 2011 to 2020. The labels indicate the element studied/optimized/compared in terms of radiation resistance by [4–6,10,13,14,16,21–23,31–33,35–37,53–56]. It should be noticed that the substrate may be present between the BSF and the rear contact. Note: The reader is referred to the reference list to see the exact concentration of each element in the compounds.

responsible for the cell's degradation. In this regard, the use of BRs has been extensively proposed to be able to reduce the GaAs thickness and accordingly increase the radiation tolerance while keeping practically the same current density. However, even when the remaining efficiency of the GaAs-based PV-cells after being radiated by nuclei particles is higher in PV-cells with BRs compared to those without BRs (after a specific dose of radiation since usually the BOL efficiency is lower in PV-cells with BRs), it has been mentioned in some studies that the GaAs-based subcell is still the layer with the quickest degrading parameters.

2. The stopping process that particles face throughout the PV-cell with highly electronic bonding structure directionality, *e.g.*, GaInP, is not fully understood yet. Thus, more study is required in this regard.
3. Degradation of interfaces among the cell's layers due to the fluence of particles has been proposed in many studies. However, a fully satisfactory physical modeling is still missing.
4. The degradation study of PV-cells due to the bombardment of nuclei particles at extreme low/high temperatures and solar irradiances is still quite limited. Such conditions are of huge interest for future space exploration missions. In this respect, more studies should be done in this direction.
5. Some studies suggest that the PV-cell's shunt-resistance is reduced after radiation based on the presence of the typical slope in the IV-characteristics or based on the FF reduction. However, other studies believe that such a slope in the IV-characteristics after radiation is due to a voltage dependency of the photo-generated current. Therefore, more theoretical and experimental studies are required to determine the actual nature of this effect.

4. Conclusion

The present paper reviewed some important studies dedicated to the analysis of radiation-induced degradation mechanisms of III–V PV-cells following a chronological approach. The main aspects of different studies and their contributions were carefully reviewed and the most significant mathematical approximations used for radiation-induced degradation modeling of PV-cells were introduced. Besides, the main characteristics and outcomes of the reported experiments and simulation studies were provided and several important remarks related to degradation analysis of PV-cells for a wide range of architectures and materials were addressed. The study concluded with some important challenges that are still open for more investigation to facilitate the development of more optimal PV-cells for future deep space explorations.

CRediT authorship contribution statement

José Maurilio Raya-Armenta: Conceptualization of this study, Methodology, Software, Writing – original draft. **Najmeh Bazmohammadi:** Supervision, Revision, Writing – original draft. **Juan C. Vasquez:** Supervision, Revision. **Josep M. Guerrero:** Conceptualization of this study, Supervision, Revision.

Declaration of competing interest

The authors declare that they have no known competing financial interests or personal relationships that could have appeared to influence the work reported in this paper.

Acknowledgments

This work was supported by the Mexican National Council of Science and Technology (CONACYT) [scholarship number 709940]; the research work was funded also by a Villum Investigator grant (no. 25920) from The Villum Fonden, Denmark; and partly sponsored by the Universidad de la Salle Bajío, Guanajuato, México.

Appendix. Description of variables

List of Symbols

α	Optical absorption coefficient.
δ_n	Excess electron concentration.
δ_p	Excess holes concentration.
ϵ	Relative permittivity.
ϵ_0	Permittivity of vacuum.
η_{EQE}	External quantum efficiency.
λ	Wavelength.
μ_n	Mobility of electrons.
Φ	Photogeneration rate.
ϕ	Particle fluence.
ϕ'	Average potential gradient in the p–n junction.
Φ_0	Photon flux.
σ_i	Capture cross section of minority-carriers by recombination centers.
σ_{niel}	Interaction cross section.
τ	Minority carrier lifetime.
τ_0	Initial minority carrier lifetime.
τ_B	Band to band recombination lifetime.
τ_n	Electrons lifetime.
τ_p	Holes lifetime.
τ_r	Radiative recombination time.
τ_{Aug}	Auger recombination lifetime.
τ_{bulk}	Minority-carrier lifetime in the bulk.
τ_{eff}	Effective minority-carrier lifetime considering the bulk and surface influences.
τ_{id}	Minority carrier lifetime associated to the newly-introduced defects.
τ_{nr}	Non-radiative recombination time.
τ_{SRH}	Trap-assisted recombination lifetime (Shockley–Read-Hall).
τ_{surf}	Minority-carrier lifetime in the surface.
φ_{EL}	Electroluminescence intensity.
A_0	Initial effective area of the cell.
A_s	Solar cell surface.
$A_{1-x}B_x$	Composition of the alloy material.
A_{ef}	Effective area of the cell.
B_{bb}	Band to band recombination coefficient.
c	Speed of light.
C_n	Recombination coefficient of electrons.
C_p	Recombination coefficient of holes.
C_{Aug}	Auger recombination coefficient.
D	Minority-carrier diffusion coefficient.
d	Cell thickness.
d_B	Thickness of the base quasi-neutral region.
d_E	Thickness of the emitter quasi-neutral region.
D_n	Electron diffusion coefficient.
D_p	Hole diffusion coefficient.
D_{ddd}	Displacement damage dose.
D_{it}	Interface trap density.
E	Energy.
E_g	Material bandgap energy.
$E_g(A)$	Bandgap energy of material A.
$f(E_{tj})$	Capture rate of majority-carriers by trap centers.
F_λ	Spectral photon flux.
F_{bb}	Photon flux of black body.
f_{FR}	Photon recycling factor.
G	Energy partition function.
G_p	Conductance.
h	Planck constant.
I_r	Recombination current.
I_{ph}	Photo-generated current.
I_{ri}	Introduction rate of recombination centers.
I_{sc}	Short-circuit current of a cell.
I_{tj}	Introduction rate of majority-carrier trap centers by electron irradiation.
J_0	Dark saturation current density.
J_D	Contribution of the depletion layer to the J_{sc}.
J_{sc}	Short-circuit current density.
k	Boltzmann constant.
K_L	Damage coefficient for minority-carrier diffusion length.
K_n	Damage coefficient for the SRV at the base-BSF interface.
K_p	Damage coefficient for the SRV at the window-emitter interface.
K_R	Damage coefficient for minority-carrier lifetime.
k_R	Irradiation-induced defect recombination coefficient.
L	Minority-carrier diffusion length.
L_n	Diffusion length of electrons.
L_p	Diffusion length of holes.
n	Ideality factor.
n'	Statistical factor of Shockley–Read theory.
N_a	Acceptors concentration.
n_a	Atomic density of the target material.
N_c	Effective density of states in the conduction band.
N_d	Donors concentration.
n_i	Intrinsic electron concentration.
N_R	Recombination center density.
N_t	Concentration of deep-level traps.
N_v	Effective density of states in the valence band.
$n_{i,B}$	Intrinsic carrier concentration in the base.
$n_{i,E}$	Intrinsic carrier concentration in the emitter.
p	Concentration of holes.
p'	Statistical factor of Shockley–Read theory.
p_i	Intrinsic holes concentration.
P_m	Maximum point of power.
Q	Kinetic energy of the recoil.
q	Elementary charge.
Q_{max}	Maximum kinetic energy that can be given to a recoil by a particle of energy E.
r	Radius of the cylindrical volume.
R_c	Carrier removal rate.
R_e	Relative damage coefficient of electrons.
R_p	Relative damage coefficient of protons.
R_{RAD}	Radiative recombination rate.
R_{REC}	Recombination rate.
S	Non-ionizing energy loss.
S_F	Front surface recombination velocity.
S_n	Surface recombination velocity at the base-BSF interface.
S_p	Surface recombination velocity at the window-emitter interface.
S_R	Rear surface recombination velocity.
S_{AM0}	AM0 solar spectrum irradiance.
S_{eff}	Effective surface recombination velocity.
SR	Spectral response.
T	Cell temperature.
T_d	Threshold energy to displace an atom.
V	Cell voltage.
v	Thermal velocity of minority-carriers.
V_T	Thermal voltage.
V_{bi}	Built-in voltage.
V_{oc}	Open-circuit voltage.
W	Width of the depletion region.

w	Frequency.
W_{wafer}	Wafer thickness.
x_1	Emitter thickness.
A, a, B, b	Constants for the range across the coverglass.
P	Alloy-dependent material.

References

[61] H. Tada, J. Carter Jr, B. Anspaugh, D. R.G., Solar Cell Radiation Handbook - Third Edition, Technical Report, Jet Propulsion Laboratory, 1982, URL: https://ntrs.nasa.gov/citations/19830006416.

[46] B. Anspaugh, et al., GaAs Solar Cell Radiation Handbook, Technical Report, National Aeronautics and Space Administration, Jet Propulsion Laboratory, 1996, URL: https://ntrs.nasa.gov/citations/19970010878.

[9] S.R. Messenger, G.P. Summers, E.A. Burke, R.J. Walters, M.A. Xapsos, Modeling solar cell degradation in space: A comparison of the nrl displacement damage dose and the JPL equivalent fluence approaches, Prog. Photovolt., Res. Appl. 9 (2) (2001) 103–121, http://dx.doi.org/10.1002/pip.357.

[1] E.F. Lisbona, Llf-2 - calibration, testing and monitoring of space solar cells, in: T. Markvart, L.C. ner (Eds.), Solar Cells, Elsevier Science, Oxford, 2005, pp. 475–503, http://dx.doi.org/10.1016/B978-185617457-2/50019-6, URL: https://www.sciencedirect.com/science/article/pii/B9781856174572500196.

[2] D.C. Jordan, S.R. Kurtz, Photovoltaic degradation rates—An analytical review, Prog. Photovolt., Res. Appl. 21 (1) (2013) 12–29, http://dx.doi.org/10.1002/pip.1182.

[3] T. Torchynska, G. Polupan, III-V material solar cells for space application, Semicond. Phys. Quantum Electron. Optoelectron. (2002) 063–070, http://dx.doi.org/10.15407/spqeo5.01.063.

[4] N. Gruginskie, F. Cappelluti, G.J. Bauhuis, P. Mulder, E.J. Haverkamp, E. Vlieg, J.J. Schermer, Electron radiation–induced degradation of GaAs solar cells with different architectures, Prog. Photovolt., Res. Appl. 28 (4) (2020) 266–278, http://dx.doi.org/10.1002/pip.3224.

[5] M. Salzberger, M. Rutzinger, C. Nömayr, P. Lugli, C.G. Zimmermann, Voltage-dependent photocurrent in irradiated GaAs solar cells, Prog. Photovolt., Res. Appl. 26 (5) (2018) 317–323, http://dx.doi.org/10.1002/pip.2983.

[6] S.I. Maximenko, M.P. Lumb, J. Moore, L.C. Hirst, M.K. Yakes, P.P. Jenkins, Thin GaAs solar cells for high irradiation levels, in: 2019 IEEE 46th Photovoltaic Specialists Conference (PVSC), 2019, pp. 2814–2817, http://dx.doi.org/10.1109/PVSC40753.2019.8980879.

[7] N. Gruginskie, F. Cappelluti, M. van Eerden, G. Bauhuis, P. Mulder, E. Vlieg, J. Schermer, Proton irradiation induced GaAs solar cell performance degradation simulations using a physics-based model, Sol. Energy Mater. Sol. Cells 223 (2021) 110971, http://dx.doi.org/10.1016/j.solmat.2021.110971.

[8] S.R. Messenger, E.A. Burke, R.J. Walters, J.H. Warner, G.P. Summers, T.L. Morton, Effect of omnidirectional proton irradiation on shielded solar cells, IEEE Trans. Nucl. Sci. 53 (6) (2006) 3771–3778, http://dx.doi.org/10.1109/TNS.2006.886220.

[10] C. Weiss, S. Park, J. Lefèvre, B. Boizot, C. Mohr, O. Cavani, S. Picard, R. Kurstjens, T. Niewelt, S. Janz, Electron and proton irradiation effect on the minority carrier lifetime in SiC passivated p-doped ge wafers for space photovoltaics, Sol. Energy Mater. Sol. Cells 209 (2020) 110430, http://dx.doi.org/10.1016/j.solmat.2020.110430.

[11] W. Rong, L. Yunhong, S. Xufang, Effects of 0.28–2.80MeV proton irradiation on GaInP/GaAs/Ge triple-junction solar cells for space use, Nucl. Instrum. Methods Phys. Res. B 266 (5) (2008) 745–749, http://dx.doi.org/10.1016/j.nimb.2007.12.076.

[12] S.J. Taylor, M. Yamaguchi, T. Yamaguchi, S. Watanabe, K. Ando, S. Matsuda, T. Hisamatsu, S.I. Kim, Comparison of the effects of electron and proton irradiation on n+–p–p+ silicon diodes, J. Appl. Phys. 83 (9) (1998) 4620–4627, http://dx.doi.org/10.1063/1.367246.

[13] A. Aierken, L. Fang, M. Heini, Q. Zhang, Z. Li, X. Zhao, M. Sailai, H. Liu, Q. Guo, W. Gao, H. Gao, Q. Sun, Effects of proton irradiation on upright metamorphic GaInP/GaInAs/Ge triple junction solar cells, Sol. Energy Mater. Sol. Cells 185 (2018) 36–44, http://dx.doi.org/10.1016/j.solmat.2018.04.035.

[14] X. Zhao, A. Aierken, M. Heini, M. Tan, Y. Wu, S. Lu, R. Hao, J. Mo, Y. Zhuang, X. Shen, Y. Xu, Q. Lei, Q. Guo, Degradation characteristics of electron and proton irradiated InGaAsP/InGaAs dual junction solar cell, Sol. Energy Mater. Sol. Cells 206 (2020) 110339, http://dx.doi.org/10.1016/j.solmat.2019.110339.

[15] S.Z. Karazhanov, Mechanism for the anomalous degradation of silicon space solar cells, Appl. Phys. Lett. 76 (19) (2000) 2689–2691, http://dx.doi.org/10.1063/1.126445.

[16] S. Park, J.C. Bourgoin, H. Sim, C. Baur, V. Khorenko, O. Cavani, J. Bourcois, S. Picard, B. Boizot, Space degradation of 3J solar cells: I—Proton irradiation, Prog. Photovolt., Res. Appl. 26 (10) (2018) 778–788, http://dx.doi.org/10.1002/pip.3016.

[17] M. Yamaguchi, S.J. Taylor, S. Matsuda, O. Kawasaki, Mechanism for the anomalous degradation of Si solar cells induced by high fluence 1 MeV electron irradiation, Appl. Phys. Lett. 68 (22) (1996) 3141–3143, http://dx.doi.org/10.1063/1.115804.

[18] M. Imaizumi, M. Yamaguchi, S. Taylor, S. Matsuda, O. Kawasaki, T. Hisamatsu, Mechanism for the anomalous degradation of Si solar cells induced by high-energy proton irradiation, Sol. Energy Mater. Sol. Cells 50 (1) (1998) 339–344, http://dx.doi.org/10.1016/S0927-0248(97)00164-5.

[19] S.-i. Sato, T. Ohshima, M. Imaizumi, Modeling of degradation behavior of InGaP/GaAs/Ge triple-junction space solar cell exposed to charged particles, J. Appl. Phys. 105 (4) (2009) 044504, http://dx.doi.org/10.1063/1.3079522.

[20] S. ichiro Sato, H. Miyamoto, M. Imaizumi, K. Shimazaki, C. Morioka, K. Kawano, T. Ohshima, Degradation modeling of InGaP/GaAs/Ge triple-junction solar cells irradiated with various-energy protons, Sol. Energy Mater. Sol. Cells 93 (6) (2009) 768–773, http://dx.doi.org/10.1016/j.solmat.2008.09.044, 17th International Photovoltaic Science and Engineering Conference.

[21] G. Hongliang, S. Linfeng, S. Qiang, Z. Qiming, W. Yiyong, X. Jingdong, G. Bin, Z. Yanqing, Degradation of up-grown metamorphic InGaP/InGaAs/Ge solar cells by low-energy proton irradiation, Sol. Energy Mater. Sol. Cells 191 (2019) 399–405, http://dx.doi.org/10.1016/j.solmat.2018.11.033.

[22] R. Lang, J. Schön, J. Lefèvre, B. Boizot, F. Dimroth, D. Lackner, Radiation hardness and post irradiation regeneration behavior of GaInAsP solar cells, Sol. Energy Mater. Sol. Cells 211 (2020) 110551, http://dx.doi.org/10.1016/j.solmat.2020.110551.

[23] G. Yan, J. ling Wang, J. Liu, Y. yu Liu, R. Wu, R. Wang, Electroluminescence analysis of VOC degradation of individual subcell in GaInP/GaAs/Ge space solar cells irradiated by 1.0 MeV electrons, J. Lumin. 219 (2020) 116905, http://dx.doi.org/10.1016/j.jlumin.2019.116905.

[24] T. Takamoto, M. Yamaguchi, S.J. Taylor, M.-J. Yang, E. Ikeda, H. Kurita, Radiation resistance of high-efficiency InGaP/GaAs tandem solar cells, Sol. Energy Mater. Sol. Cells 58 (3) (1999) 265–276, http://dx.doi.org/10.1016/S0927-0248(99)00003-3.

[25] G.P. Summers, S.R. Messenger, E.A. Burke, M.A. Xapsos, R.J. Walters, Contribution of low-energy protons to the degradation of shielded GaAs solar cells in space, Prog. Photovolt., Res. Appl. 5 (6) (1997) 407–413, http://dx.doi.org/10.1002/(SICI)1099-159X(199711/12)5:6<407::AID-PIP192>3.0.CO;2-P.

[26] N.Z. Vagidov, K.H. Montgomery, G.K. Bradshaw, D.A. Wilt, Light trapping structures for radiation hardness enhancement of space solar cells, Sol. Energy Mater. Sol. Cells 182 (2018) 136–141, http://dx.doi.org/10.1016/j.solmat.2018.03.036.

[27] S. Tobin, S. Vernon, M. Sanfacon, A. Mastrovito, Enhanced light absorption in GaAs solar cells with internal Bragg reflectors, in: The Conference Record of the Twenty-Second IEEE Photovoltaic Specialists Conference - 1991, 1991, pp. 147–152 vol.1, http://dx.doi.org/10.1109/PVSC.1991.169199.

[28] S.R. Messenger, E.M. Jackson, J.H. Warner, R.J. Walters, Scream: A new code for solar cell degradation prediction using the displacement damage dose approach, in: 2010 35th IEEE Photovoltaic Specialists Conference, 2010, pp. 001106–001111, http://dx.doi.org/10.1109/PVSC.2010.5614713.

[29] M. Yamaguchi, A. Khan, S.J. Taylor, M. Imaizumi, T. Hisamatsu, S. Matsuda, A detailed model to improve the radiation-resistance of Si space solar cells, IEEE Trans. Electron Devices 46 (10) (1999) 2133–2138, http://dx.doi.org/10.1109/16.792008.

[30] M. Zazoui, J.C. Bourgoin, Space degradation of multijunction solar cells: An electroluminescence study, Appl. Phys. Lett. 80 (23) (2002) 4455–4457, http://dx.doi.org/10.1063/1.1485134.

[31] C. Peng, F. Ding, Z. Lei, Z. Zhang, Y. En, Y. Huang, Investigation of radiation-induced degradations in four-junction solar cell by experiment and simulation, Microelectron. Reliab. 108 (2020) 113646, http://dx.doi.org/10.1016/j.microrel.2020.113646.

[32] T. Takamoto, H. Washio, H. Juso, Application of InGaP/GaAs/Ingaas triple junction solar cells to space use and concentrator photovoltaic, in: 2014 IEEE 40th Photovoltaic Specialist Conference (PVSC), 2014, pp. 0001–0005, http://dx.doi.org/10.1109/PVSC.2014.6924936.

[33] H. Gao, R. Yang, Y. Zhang, Improving radiation resistance of GaInP/GaInAs/Ge triple-junction solar cells using GaInP back-surface field in the middle subcell, Materials 13 (8) (2020) http://dx.doi.org/10.3390/ma13081958.

[34] W. Laiadi, A. Meftah, C. Laiadi, Effect of proton irradiation fluence on the performance of the AlxGa1-xAs/GaAs p+ nn+ solar cell, Algerian J. Environ. Sci. Technol. 7 (3) (2021) https://www.aljest.org/index.php/aljest/article/view/580.

[35] V.M. Lantratov, V.M. Emelyanov, N.A. Kalyuzhnyy, S.A. Mintairov, M.Z. Shvarts, Improvement of radiation resistance of multijunction GaInP/Ga(In)As/Ge solar cells with application of bragg reflectors, in: 5th Forum on New Materials Part C, in: Advances in Science and Technology, vol. 74, Trans Tech Publications Ltd, 2011, pp. 225–230, http://dx.doi.org/10.4028/www.scientific.net/AST.74.225.

[36] S.J. Polly, G.T. Nelson, J.R. D'Rozario, R. Tatavarti, S.M. Hubbard, Radiation effects in thinned GaAs photovoltaics incorporating DBRs for improved radiation tolerance of multijunctions, in: 2019 IEEE 46th Photovoltaic Specialists Conference (PVSC), 2019, pp. 2818–2821, http://dx.doi.org/10.1109/PVSC40753.2019.8980875.

[37] R. Tatavarti, K. Forghani, R. Reddy, J.R. D'Rozario, G.T. Nelson, S. Hubbard, Radiation hardening of dual junction solar cells, in: 2020 47th IEEE Photovoltaic Specialists Conference (PVSC), 2020, pp. 2258–2261, http://dx.doi.org/10.1109/PVSC45281.2020.9300545.

[38] R.R. King, D.C. Law, K.M. Edmondson, C.M. Fetzer, G.S. Kinsey, H. Yoon, R.A. Sherif, N.H. Karam, 40% efficient metamorphic GaInP/GaInAs/Ge multijunction solar cells, Appl. Phys. Lett. 90 (18) (2007) 183516, http://dx.doi.org/10.1063/1.2734507.

[39] W. Guter, J. Schöne, S.P. Philipps, M. Steiner, G. Siefer, A. Wekkeli, E. Welser, E. Oliva, A.W. Bett, F. Dimroth, Current-matched triple-junction solar cell reaching 41.1% conversion efficiency under concentrated sunlight, Appl. Phys. Lett. 94 (22) (2009) 223504, http://dx.doi.org/10.1063/1.3148341.

[40] D.J. Curtin, R.L. Statler, Review of radiation damage to silicon solar cells, IEEE Trans. Aerosp. Electron. Syst. AES-11 (4) (1975) 499–513, http://dx.doi.org/10.1109/TAES.1975.308112.

[41] R. Hill, N.M. Pearsall, Indium phosphide solar cells, in: IEE Colloquium on Solar Cells for Space Applications, 1988, pp. 2/1–2/5, URL: https://ieeexplore.ieee.org/document/209641.

[42] J.R. Woodyard, G.A. Landis, Radiation resistance of thin-film solar cells for space photovoltaic power, Sol. Cells 31 (4) (1991) 297–329, http://dx.doi.org/10.1016/0379-6787(91)90103-V, Special Issue: Radiation Effects on Solar Cells.

[43] R.J. Walters, A review of radiation effects in InP solar cells, in: Proceedings of 1994 IEEE 6th International Conference on Indium Phosphide and Related Materials (IPRM), 1994, pp. 275–279, http://dx.doi.org/10.1109/ICIPRM.1994.328220.

[44] J. Li, A. Aierken, Y. Liu, Y. Zhuang, X. Yang, J.H. Mo, R.K. Fan, Q.Y. Chen, S.Y. Zhang, Y.M. Huang, Q. Zhang, A brief review of high efficiency III-V solar cells for space application, Front. Phys. 8 (2021) 657, http://dx.doi.org/10.3389/fphy.2020.631925.

[45] B. Anspaugh, Proton and electron damage coefficients for GaAs/Ge solar cells, in: The Conference Record of the Twenty-Second IEEE Photovoltaic Specialists Conference - 1991, Vol.2, 1991, pp. 1593–1598, http://dx.doi.org/10.1109/PVSC.1991.169472.

[47] S. Karazhanov, Mechanism for the anomalous degradation of proton- or electron-irradiated silicon solar cells, Sol. Energy Mater. Sol. Cells 69 (1) (2001) 53–60, http://dx.doi.org/10.1016/S0927-0248(00)00358-5.

[48] N. de Angelis, J. Bourgoin, T. Takamoto, A. Khan, M. Yamaguchi, Solar cell degradation by electron irradiation. Comparison between Si, GaAs and GaInP cells, Sol. Energy Mater. Sol. Cells 66 (1) (2001) 495–500, http://dx.doi.org/10.1016/S0927-0248(00)00211-7, PVSEC 11 - Part II.

[49] S.R. Messenger, E.A. Burke, T.L. Morton, G.P. Summers, R.J. Walters, J.H. Warner, Modelling low energy proton radiation effects on solar cells, in: 3rd World Conference on Photovoltaic Energy Conversion, 2003. Proceedings of, Vol. 1, 2003, pp. 716–719, URL: https://ieeexplore.ieee.org/abstract/document/1305382.

[50] T. Sumita, M. Imaizumi, S. Matsuda, T. Ohshima, A. Ohi, H. Itoh, Proton radiation analysis of multi-junction space solar cells, Nucl. Instrum. Methods Phys. Res. B 206 (2003) 448–451, http://dx.doi.org/10.1016/S0168-583X(03)00791-2, 13th International Conference on Ion Beam Modification of Materials.

[51] S. Makham, M. Zazoui, G. Sun, J. Bourgoin, Prediction of proton-induced degradation of GaAs space solar cells, Sol. Energy Mater. Sol. Cells 90 (10) (2006) 1513–1518, http://dx.doi.org/10.1016/j.solmat.2005.10.015, Selected Papers from the 8th International Conference on Condensed Matter and Statistical Physics.

[52] V. Emelyanov, N. Kalyuzhniy, S. Mintairov, M. Shvarts, V. Lantratov, Multijunction GaInP/GaInAs/Ge solar cells with Bragg reflectors, Semiconductors 44 (12) (2010) 1600–1605, http://dx.doi.org/10.1134/S1063782610120122.

[53] M.Z. Shvarts, E.A. Aronova, V.M. Emelyanov, N.A. Kalyuzhnyy, V.M. Lantratov, S.A. Mintairov, A.A. Soluyanov, N.K. Timoshina, Multijunction solar cell with intermediate IR reflector, AIP Conf. Proc. 1477 (1) (2012) 28–31, http://dx.doi.org/10.1063/1.4753826.

[54] A. Skachkov, Optimization of the structure of a GaInP/GaAs/Ge triple-junction solar cell with an Al 0.1 Ga 0.9 As/Al 0.8 Ga 0.2 As integrated bragg reflector, Optoelectron. Instrum. Data Process. 50 (4) (2014) 423–427, http://dx.doi.org/10.3103/S8756699014040165.

[55] Y. Jiang, M.J. Keevers, P. Pearce, N. Ekins-Daukes, M.A. Green, Design of an intermediate Bragg reflector within triple-junction solar cells for spectrum splitting applications, Sol. Energy Mater. Sol. Cells 193 (2019) 259–269, http://dx.doi.org/10.1016/j.solmat.2019.01.011.

[56] H. Karadeniz, A study on triple-junction GaInP2/InGaAs/Ge space grade solar cells irradiated by 24.5 MeV high-energy protons, Nucl. Instrum. Methods Phys. Res. B 471 (2020) 1–6, http://dx.doi.org/10.1016/j.nimb.2020.03.015.

[57] E. Yaccuzzi, S.D. Napoli, E.J.D. Liscia, S. Suárez, M. Alurralde, A. Strittmatter, J. Pla, P. Giudici, Experimental re-evaluation of proton penetration ranges in GaAs and InGaP, J. Phys. D: Appl. Phys. 54 (11) (2021) 115302, http://dx.doi.org/10.1088/1361-6463/abce7d.

[58] P. Iles, Evolution of space solar cells, Sol. Energy Mater. Sol. Cells 68 (1) (2001) 1–13, http://dx.doi.org/10.1016/S0927-0248(00)00341-X, Solar cells in space.

[59] H. Tada, J. Carter Jr, Solar Cell Radiation Handbook, Technical Report, Jet Propulsion Laboratory, 1977, URL: https://ntrs.nasa.gov/citations/19780007623.

[60] A. Hadjdida, M. Bourahla, H. Ertan, B. Mohammed, Analytical modelling, simulation and comparative study of multi-junction solar cells efficiency, Int. J. Renew. Energy Res. 8 (4) (2018) 1824–1832, https://www.ijrer.org/ijrer/index.php/ijrer/article/view/8135.